NPS-57Gn72121A

NAVAL POSTGRADUATE SCHOOL

Monterey, California

GENERALIZED PERFORMANCE LIMITS
FOR PROPELLERS, WINDMILLS
AND LIFTING ROTORS WITH AXES
PARALLEL TO THE UNDISTURBED FLOW

T. H. GAWAIN, D.Sc

December 1972

NAVAL POSTGRADUATE SCHOOL

Monterey, California

Rear Admiral Mason Freeman, USN
Superintendent

Milton U. Clauser
Provost

ABSTRACT:

This paper generalizes the classical momentum theory as usually applied to propellers,windmills and lifting rotors into a single unified treatment. It also extends the analysis to include the regime in which flow through part or all of the actuator disc is reversed with respect to the remote flow field. Dimensional analysis is used in a systematic manner to reduce the final results to their simplest and most significant forms. It is shown that the performance of these devices can always be represented by a single parameter family of curves in which the parameter expresses the extent to which the performance of the actual device falls short of the theoretical limit. Detailed algebraic solutions are derived in closed form for the performance of both the idealized zero torque and finite torque actuators; these represent performance limits which any comparable real device may approach but never exceed. A qualitative analysis is presented concerning the development of the vortex ring state. The fundamental dynamic stability of the ideal lifting rotor is also analyzed.

While this paper deals with a classical topic in fundamental fluid mechanics, the approach employed is original and many of the results derived here are in a form that is essentially new. In particular, the solutions obtained for the reversed and transition flow regimes and for the idealized rotating actuator are believed to represent new formulations of these basic phenomena.

TABLE OF CONTENTS

TABLES

FIGURES

1. Objectives of the Analysis

The simple actuator disc has long served as a useful idealization and standard of comparison for the performance, within a certain restricted operating range, of a broad class of fluid-mechanical devices. These include the ordinary aircraft propeller, the lifting rotor such as the helicopter rotor under certain conditions of vertical ascent or descent, and the unshrouded axial flow turbine or "windmill" as it is termed in this paper. The fundamental analysis presented here is applicable to all three of these devices which we designate here collectively as "actuators."

The chief purpose of the present analysis is to extend the elementary and classical momentum theory of the idealized actuator so as the obtain theoretical performance limits over the entire possible operating range, including the regime in which the flow through part or all of the actuator disc is reversed with respect to the remote flow field! In all cases considered in this paper, however, the axis of the actuator remains parallel to the undisturbed flow far away.

Another purpose of this paper is to utilize dimensional analysis in a systematic manner to reduce the final results to their simplest and most significant forms. It will be shown, in particular, that the performance of any of the foregoing devices can always be represented by a single parameter family of curves; this parameter expresses the extent to which performance of the actual device falls short of the limit theoretically attainable from the comparable ideal actuator.

This paper also considers certain fundamental aspects of the dynamic and hydrodynamic stability of the ideal actuator.

2. Summary of Principal Concepts, Equations and Generalized Performance Charts

The main results of this analysis are summarized in subsections 2.1 through 2.11 inclusive. The detailed derivations are given elsewhere in this paper, but enough information is included in these subsections to define all results without the need to refer to the actual derivations.

2.1 Nomenclature for Section 2

All symbols which occur in the summary of principal results, subsections 2.2 through 2.11 inclusive, are defined in the text when first mentioned and also, for ease of reference, in the summary below. Symbols are listed below according to the subsection and in the approximate order in which they are introduced in the text. A dash -- after the definition signifies that the quantity is dimensionless.

Subsection 2.2

F = force exerted by actuator upon fluid, positive if in the same sense as the velocity of the undisturbed fluid. lbf

L = reaction exerted by the fluid upon a lifting rotor, always upward and positive by definition. lbf

V = axial velocity of undisturbed fluid relative to actuator disc, always non-negative by definition. ft/sec

$\dot{H}$ = rate of vertical climb of a lifting rotor, positive upward. ft/sec

τ = sign changing operator defined by Eq. (2.2.3). --

Subsection 2.3

ρ = fluid density (constant). slugs/ft^3

D = diameter of actuator. ft

P_i = shaft power of an ideal actuator, positive if supplied to actuator. ft lbf/sec

P = actual shaft power, positive if supplied to actuator. ft lbf/sec

P_f = power loss due to all non-ideal effects, always non-negative. ft lbf/sec

N = shaft rotational speed, positive by definition. rev/sec

μ = fluid viscosity. lbf sec/ft^2

Subsection 2.4

Note: All dimensionless coefficients listed immediately below are defined mathematically in Table 2.4.1.

C_F = conventional force coefficient in ρ, N, D system. --

C_P = conventional power coefficient in ρ, N, D system. --

J = conventional advance ratio in ρ, N, D system. --

C_{P_f} = power loss coefficient in ρ, N, D system. --

C_{1F}, C_{1P}, C_{1N}, C_{1P_f} = performance coefficients in the ρ, D, V system. --

C_{2F}, C_{2V}, C_{2N}, C_{2P_f} = performance coefficients in the ρ, D, $|P|$ system. --

C_{3P}, $C_{3\dot{H}}$, C_{3N}, C_{3P_f} = performance coefficients in the ρ, D, L system. --

Subsection 2.5

V_d = axial velocity at actuator disc, positive if in the same sense as the undisturbed flow. ft/sec

φ, τ, σ_i, σ = sign changing operators defined by Eqs. (2.5). --

Subsection 2.6

P, W, T, R = symbols denoting propulsive, windmill, transition and reversed flow operating modes, respectively.

M = symbol denoting operating point which corresponds to generation of maximum possible windmill power $|C_{1P}|$.

B = symbol denoting operating point which corresponds to maximum drag force at zero net shaft power.

α,m = parameters occurring in the cubic solution for thrust coefficient as defined in Eq. (2.6.4) of Table 2.6.2. --

Subsection 2.7

TR, TW = symbols denoting subregions of the transition mode corresponding, respectively, to positive and negative net shaft power.

α, m = parameters occurring in the cubic solution for thrust coefficient as defined in Eq. (2.7.7) of Table 2.7.4. --

β = parameter occurring in the cubic solution for velocity coefficient as defined in Eq. (2.7.7) of Table 2.7.4. --

Subsection 2.8

S = symbol denoting operating point which corresponds to static conditions (V = 0).

δ = parameter occurring in the cubic solution for rate of descent at zero power as defined in Note 2 of Table 2.8.1. --

Subsection 2.9

r_0 = radius of non-swirling core in remote slipstream. ft

$C_F)_{MAX}$, $C_P)_{MAX}$ = maximum values of conventional thrust and power coefficients that can be attained at any specified advance ratio J by an idealized finite torque actuator. --

R = slipstream radius. ft

r = slipstream radial coordinate. ft

ω = shaft angular velocity. rad/sec

V_S = slipstream axial velocity. ft/sec

V_u = slipstream peripheral velocity. ft/sec

Γ = slipstream vortex strength outside core region. ft^2/sec

μ = slipstream advance ratio defined by Eq. (2.9.2) of Table 2.9.1. --

Λ = slipstream loading parameter defined by Eq. (2.9.3) of Table 2.9.1. --

γ = slipstream swirl parameter defined by Eq. (2.9.4) of Table 2.9.1. --

η_0 = relative radius of non-swirling core as defined by Eq. (2.9.5) of Table 2.9.1. --

ζ = auxiliary function defined by Eq. (2.9.7) of Table 2.9.1. --

Subsection 2.10

δL = perturbation in lift. lbf

W = total weight of rotorcraft. lbf

t = time coordinate. sec

θ = dimensionless time coordinate defined by Eq. (2.10.4) of Table 2.10.1. --

C_{3P}, $C_{3\dot{H}}$, C_{3L} = dimensionless performance coefficients in ρ, D, W system as defined by Eqs. (2.10.1) through (2.10.3) of Table 2.10.1. --

X, Y = dimensionless stability derivatives defined by Eqs (2.10.5) through (2.10.8) of Table 2.10.1. --

μ, ν = perturbation acceleration and velocity response constants, respectively, of control system as defined by Eq. (2.10.9) of Table 2.10.1. --

β = exponential response rate of lifting rotor to a small perturbation. (Operation is stable if β is negative). --

2.2 The Lifting Rotor in Vertical Ascent or Descent

In dealing with the lifting rotor in vertical ascent or descent, the rotor axis is placed vertically, and the sense of the flow through the actuator is so chosen that the reaction force F exerted by the fluid upon the actuator itself, whether it be a propulsive thrust,a windmilling drag or a power-on reversed thrust, always acts upward and thereby constitutes a useful lift L. These circumstances in no way affect the flow pattern itself, nor the basic method of analysis.

It is convenient, however, to introduce two minor changes of variable when dealing specifically with the lifting rotor. In place of the usual axial force F which may be either positive or negative, we introduce the lift L which is always directed upward, and which we therefore take as positive by definition.

In place of the remote velocity V which is always non-negative by definition, we introduce the rate of climb $\dot{H}$ which is positive for vertical ascent, negative for vertical descent. (The case of slanting ascent or descent falls outside the scope of this analysis.)

The required changes of variable are simple accomplished by the substitutions

$$F = \tau L \tag{2.2.1}$$

$$V = \tau \dot{H} \tag{2.2.2}$$

where τ is a sign changing operator defined as follows, namely,

$$\tau = \frac{F}{|F|} = \pm 1 \tag{2.2.3}$$

By means of these substitutions, any result originally derived for the propeller or windmill can be converted to the corresponding result for the lifting rotor in vertical ascent or descent.

2.3 Real versus Ideal Actuators

The present analysis is based on comparing the performance of any real propeller, windmill or lifting rotor with that of a corresponding idealized zero torque actuator. As illustrated in Section 11 of this paper, the above comparison can be made in more than one way. However, the scheme outlined below appears to be by far the simplest and most versatile. Hence this is the basic method which is consistently applied throughout this paper, except for the auxiliary discussion in section 11.

In this method, the idealized actuator is arbitrarily assigned values of ρ, D, V and F which are respectively equal to those of the real device, by definition. This then suffices to fix the theoretical shaft power P_i of the ideal actuator according to a definite relation which is derived elsewhere in this paper and which can here be symbolized in the form

$$P_i = P_i\ (\rho,\ D,\ V,\ F) \qquad (2.3.1)$$

On this basis, the shaft power P of the real actuator, whether positive or negative, is always algebraically greater than the ideal shaft power P_i.

The difference between these two quantities, which we denote by symbol P_f, represents a relative loss of power due to all non-ideal effects, including those associated with slipstream rotation, viscosity, number of blades, detailed blade geometry, flow unsteadiness, separation effects and so on. Hence P_f is in general a complex function not only of ρ, D, V and F, but also of shaft speed N, of viscosity μ, and of various geometric parameters. It is necessarily non-negative. Thus symbolically,

$$P_f = P_f\ (\rho,\ V,\ D,\ F,\ N,\ \mu,\ \text{-----}) \geq 0 \qquad (2.3.2)$$

Therefore the shaft power P of the real actuator may finally be represented in the form

$$P = P_i + P_f \qquad (2.3.3)$$

Since the principal aim of this paper is to establish a <u>simple</u> performance limit which any real actuator can approach but never exceed, attention is focussed primarily on the elementary analytical relation which is symbolized by Eq. (2.3.1) and which represents the idealized zero torque actuator itself. The more complex and obscure relation symbolized by Eq. (2.3.2), which relates the real actuator to the ideal, is defined conceptually in this paper, but is only partially analyzed. In a later section the overall power loss P_f is broken down further into a rotation loss P_N plus a residual loss P_r. Of course, the latter quantity is in principle amenable to further analysis, but this requires resort to methods which are either semi-empirical in character, or

else far more complex than those considered in this paper.

In general, for any well designed actuator operating at or near its design point, the overall power loss P_f should be comparatively small and well suited to estimation in any specific instance by accepted engineering methods based on the utilization of appropriate test data.

Attention is also invited to the role of shaft speed N in the situation. Note that power loss P_f is a function of N, as indicated in Eq. (2.3.2), but that the basic relation (2.3.1) for the ideal power P_i itself is actually independent of N! This fact is subsequently used to simplify the basic analysis in a very significant way.

2.4 Dimensionless Performance Coefficients

The analysis of any propeller, windmill or lifting rotor can be simplified and generalized by reducing all quantities and equations to non-dimensional form. Since the three fundamental dimensions of force, length and time are involved in this problem, it is necessary for this purpose to choose three of the basic parameters of the problem as dimensional reference parameters. This can be done in various ways. Four of the most important possibilities are summarized in Table 2.4.1.

By far the most commonly used system of dimensionless coefficients is that labelled the "Conventional System" in the table. This uses ρ, N and D as reference parameters and results in the three familiar coefficients commonly known as the thrust coefficient C_F, power coefficient C_P and advance ratio J, as defined in the table.

We observe, however, that while shaft speed N is a significant parameter of the overall problem, it is not involved at all in the fundamental relation of the idealized zero torque actuator as symbolized by Eq. (2.3.1). Hence, although this relation can certainly be non-dimensionalized in the conventional

Table 2.4.1 Summary of Dimensionless Performance Coefficients

	Conventional System	Alternative System #1	Alternative System #2	Alternative System #3
Preferred Application →		Windmill or Drag Brake	Propeller or Reversed Power Thruster	Lifting Rotor
Dimensional Reference Parameters →	ρ, N, D	ρ, D, V	ρ, D, $\lvert P \rvert$	ρ, D, L
Axial Force F	$C_F = \frac{F}{\rho N^2 D^4}$	$C_{1F} = \frac{F}{\rho D^2 V^2} = \frac{C_F}{J^2}$	$C_{2F} = \frac{F}{\lvert \rho D^2 P^2 \rvert^{1/3}} = \frac{C_F}{\lvert C_P \rvert^{2/3}}$	1
Shaft Power P	$C_P = \frac{P}{\rho N^3 D^5}$	$C_{1P} = \frac{P}{\rho D^2 V^3} = \frac{C_P}{J^3}$	1	$C_{3P} = \frac{P}{\frac{1}{D}\sqrt{\frac{L^3}{\rho}}} = \frac{C_P}{\lvert C_F \rvert^{3/2}}$
Axial Velocity $V \geq 0$	$J = \frac{V}{ND} \geq 0$	1	$C_{2V} = \frac{V}{\lvert P/\rho D^2 \rvert^{1/3}} = \frac{1}{\lvert C_P \rvert^{1/3}} \geq 0$	$C_{3\dot{H}} = \frac{\dot{H}}{\frac{1}{D}\sqrt{\frac{L}{\rho}}} = \frac{\tau J}{\lvert C_F \rvert^{1/2}}$
Rotational Speed $N > 0$	1	$C_{1N} = \frac{N}{V/D} = \frac{1}{J} > 0$	$C_{2N} = \frac{N}{\lvert P/\rho D^5 \rvert^{1/3}} = \frac{1}{\lvert C_P \rvert^{1/3}} > 0$	$C_{3N} = \frac{N}{\frac{1}{D^2}\sqrt{\frac{L}{\rho}}} = \frac{1}{\lvert C_F \rvert^{1/2}} > 0$
Power Loss $P_f \geq 0$	$C_{Pf} = \frac{P_f}{\rho N^3 D^5} \geq 0$	$C_{1Pf} = \frac{P_f}{\rho D^2 V^3} = \frac{C_{Pf}}{J^3} \geq 0$	$C_{2Pf} = \frac{P_f}{\lvert P \rvert} = \frac{C_{Pf}}{\lvert C_P \rvert} \geq 0$	$C_{3Pf} = \frac{P_f}{\frac{1}{D}\sqrt{\frac{L^3}{\rho}}} = \frac{C_{Pf}}{\lvert C_F \rvert^{3/2}} \geq 0$

ρ, N, D system, the results so obtained will not be expressed in terms of the fewest possible number of dimensionless parameters. In effect, the conventional system introduces an extraneous parameter N into the formulation of the basic relation (2.3.1) and thereby creates one superfluous degree of freedom.

The above complication is undesirable and can be avoided simply by dropping the conventional ρ, N, D system and adopting instead any one of the three alternative schemes shown in Table 2.4.1. Notice that the various dimensionless coefficients that occur in these alternative systems can all be expressed very simply in terms of the familiar coefficients C_F, C_P and J of the conventional system. These simple conversions are summarized in the table.

The above three basic systems are theoretically equivalent in that they all express the same underlying relationship in terms of the same number of dimensionless parameters. The respective detailed results, however, are not necessarily equally apt and convenient in every possible application. As a rule, the specific context determines which one of these three systems expresses the pertinent results in the most appropriate form.

It is also worth noting that under any circumstances in which parameter N reenters the problem in a significant way, the conventional coefficients C_F, C_P and J once again become relevant. This is true, for example, of the idealized finite torque actuator as analyzed in detail in section 9, and summarized in subsection 2.9.

2.5 Sign Changing Operators

Owing to the extremely wide range of operating conditions considered in this paper, the velocity V_d through the actuator disc, the axial force F, the ideal shaft power P_i and actual shaft power P are each subject to changes in algebraic sign. As an aid in dealing with these changes in an orderly fashion, we introduce a group of sign changing operators defined as follows:

$$\varphi = \frac{V_d}{|V_d|} = \pm 1 \tag{2.5.1}$$

$$\tau = \frac{F}{|F|} = \pm 1 \tag{2.5.2}$$

$$\sigma_i = \frac{P_i}{|P_i|} = \pm 1 \tag{2.5.3}$$

$$\sigma = \frac{P}{|P|} = \pm 1 \tag{2.5.4}$$

The usefulness of these operators for generalizing the basic analytical relations will become apparent in the following subsections.

2.6 The Basic Solution in the ρ, D, V System

The basic momentum and energy analysis shows that the complete operating envelope of an idealized zero torque actuator may be subdivided into four distinct ranges as indicated in Table 2.6.1. Each operating range has its own characteristic idealized flow pattern as shown schematically in Fig. 2.6.1. The two basic equations presented in Table 2.6.1 suffice to define the performance over this entire range. Provided only that the proper respective sign changing operators φ and τ_i be used as defined in the table, the single generalized

Table 2.6.1 Basic Actuator Performance Relations

As Functions of Force Coefficient in ρ, D, V System

Operating Mode	Symbol	Range	Sign Changing Operators		Basic Eq
			φ	σ_i	
Propulsive	P	$0 \leq C_{lF} \leq +\infty$	+1	+1	(2.6.1)
Windmill	W	$-\frac{\pi}{6}(\sqrt{3}-1) \leq C_{lF} \leq 0$	+1	-1	(2.6.1)
Transition	T	$-\frac{\pi}{6}(\sqrt{3}+1) \leq C_{lF} \leq -\frac{\pi}{6}(\sqrt{3}-1)$	Not Applicable		(2.6.2)
Reverse	R	$-\infty \leq C_{lF} \leq -\frac{\pi}{6}(\sqrt{3}+1)$	-1	+1	(2.6.1)

Basic Equations

Modes P, W and R

$$C_{lP} = \left(\frac{C_{lF}}{2}\right) + \sigma_i \sqrt{\left(\frac{C_{lF}}{2}\right)^2 + \frac{2}{\pi\varphi} C_{lF}^3} + C_{lPf} \qquad (2.6.1)$$

Mode T

$$C_{lP} = -\frac{\pi}{3\sqrt{3}} - C_{lF} + C_{lPf} \qquad (2.6.2)$$

Note: For definitions of coefficients, see Table 2.4.1.

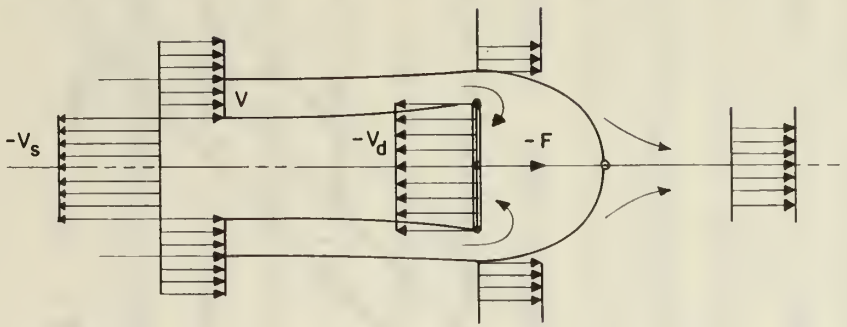

(c) REVERSED FLOW MODE R

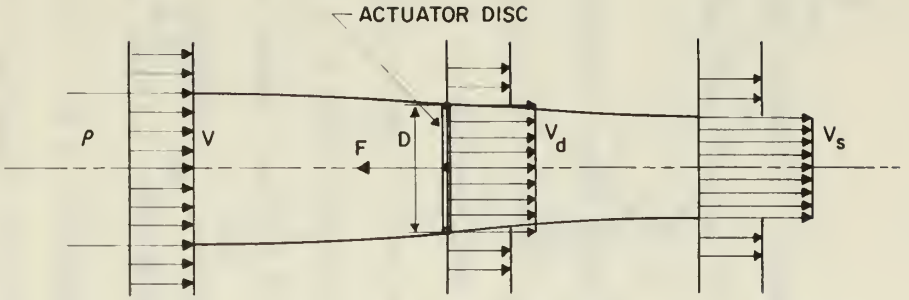

(a) PROPULSION MODE P

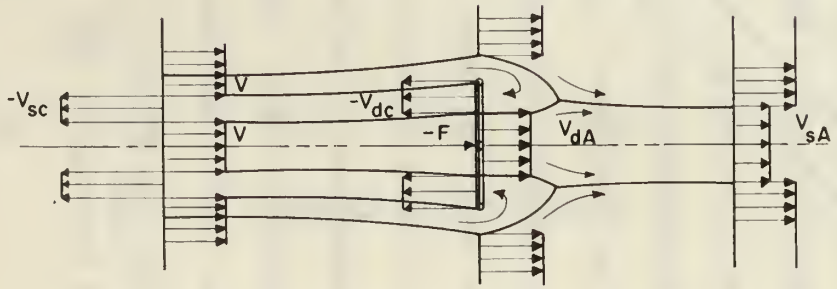

(d) TRANSITION MODE T

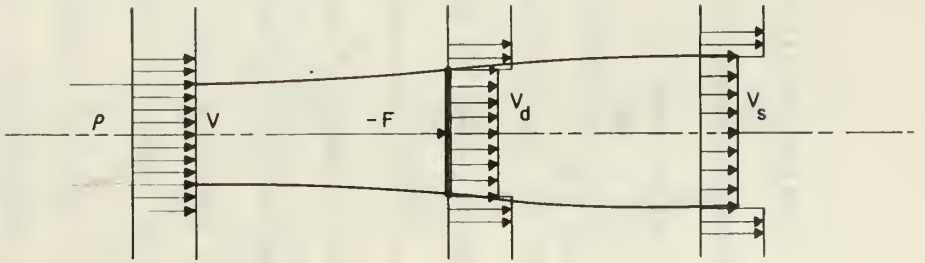

(b) WINDMILL MODE W

Fig. 2.6.1 SCHEMATIC DIAGRAMS OF OPERATING MODES.

Eq. (2.5.1) applies to all three ranges designated as modes P, W and R! The separate relation shown in Eq. (2.6.2) then applies over the remaining transition range, mode T.

Eq. (2.6.1) is completely consistent with the usual elementary momentum analysis of the simple propeller or windmill. Hence it is not surprising that the same basic result is applicable to both. But, as Fig. 2.6.1 plainly shows, the range of fully reversed flow, mode R, involves a flow pattern which seems very much more complex than the simple patterns associated with modes P or W. It is therefore perhaps surprising that Eq. (2.6.1) can include all three of these modes within a single generalized expression. In addition to generalizing the classical theory in this striking way, the present analysis also yields the novel result for the transition range as represented by Eq. (2.6.2); this particular relation has no counterpart in the usual elementary theory!

The basic overall relation defined jointly by Eqs. (2.6.1) and (2.6.2) is shown in Fig. 2.6.2 as a family of curves of C_{lP} versus C_{lF}, with C_{lPf} as parameter. The curve for $C_{lPf} = 0$ represents the ideal actuator. This defines the limiting performance which any real actuator can approach but never exceed.

The loss parameter C_{lPf} expresses quantitatively how much the performance of any real device falls short of the theoretical ideal. It also provides a convenient basis for comparing the relative performances of various real actuators.

Two critical points on the ideal curve are worthy of note. Point M shows that the magnitude of the power coefficient $|C_{lP}|$ generated by any windmill can never exceed $\frac{2\pi}{27} = 0.233$. Point B shows that the magnitude of the drag coefficient $|C_{lF}|$ which can be generated without the expenditure of net shaft power can never exceed $\frac{\pi}{3\sqrt{3}} = 0.605$. For a real actuator of specified constant C_{lPf}, these magnitudes decrease to $(\frac{2\pi}{27} - C_{lPf})$ and $(\frac{\pi}{3\sqrt{3}} - C_{lPf})$, respectively.

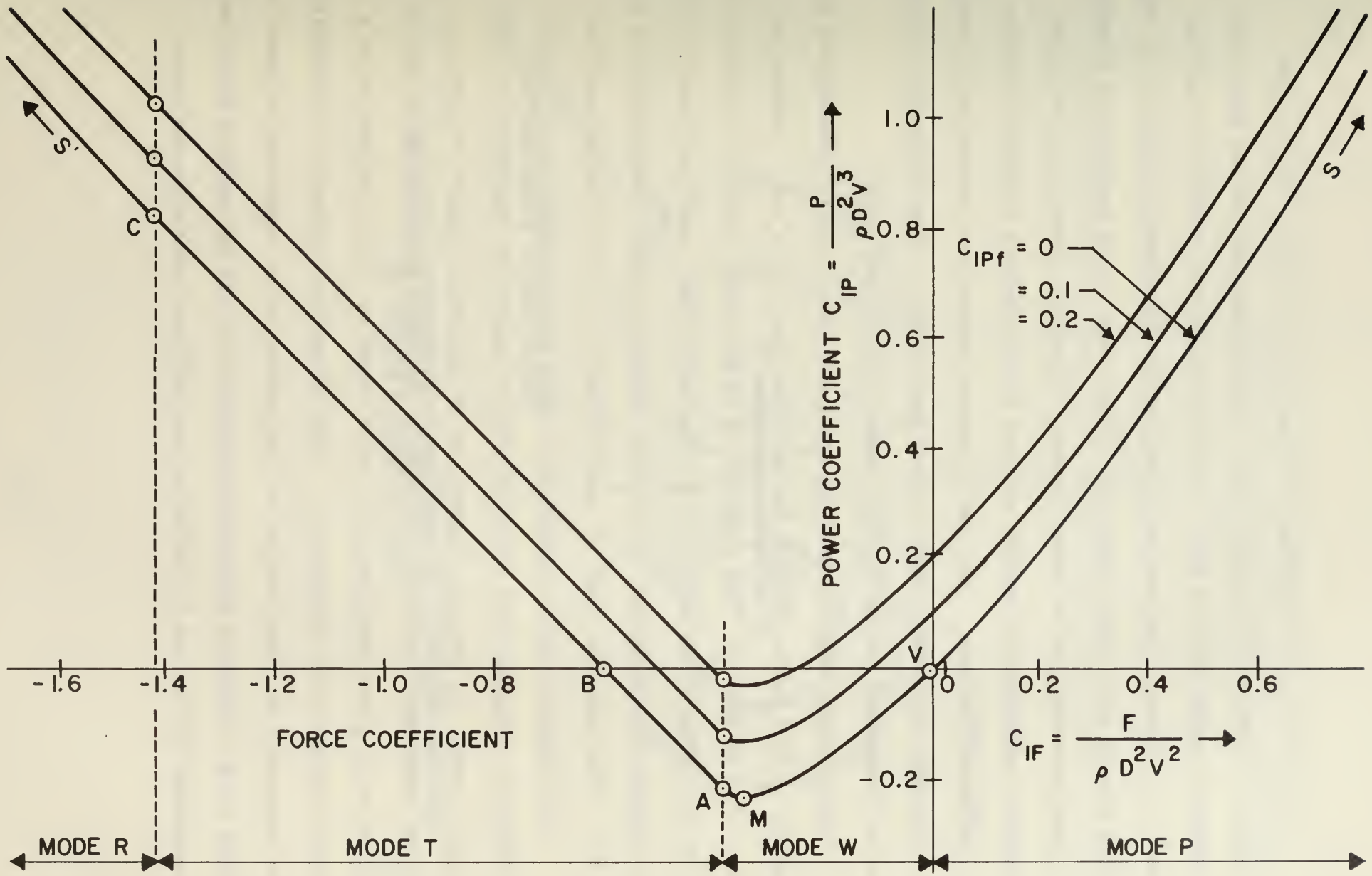

Fig. 2.6.2 BASIC ACTUATOR PERFORMANCE CURVES IN THE ρ, D, V SYSTEM.

It should be mentioned that if we set $C_{lPf} = 0$ in Eq. (2.6.1), this analytical expression can generate not only the major part of the ideal performance envelope shown in Fig. 2.6.2, but also certain extraneous solutions which if they were shown here would fall within the interior region of the chart. These details are in face shown later in Fig. 6.2. It is demonstrated elsewhere in this paper that one of these branches, although it formally satisfies the equation, represents an unstable solution which cannot be physically realized in the present context. The other extraneous branches are theoretically stable but represent performance which is less than optimal. These extraneous solutions are not considered further in this summary of principal results.

There is one singular operating condition, however, which does warrant brief comment at this point. That is the so-called ring vortex state, represented in Fig. 2.6.2 by point V. This condition is of particular interest in connection with the lifting rotor because it is associated with a catastropic loss of lift! The typical flow pattern of the vortex ring state is shown schematically in Fig. 2.6.3. This operating state is considered further in the detailed analysis.

The original solution summarized in Table 2.6.1 is based on C_{lF} as the independent variable; this choice reduces the analytical expressions to their simplest form. In practice, however, it is frequently required to take C_{lP} as the independent variable. Fortunately, the basic equations can in fact be solved for C_{lF} as a function of C_{lP}, even though Eq. (2.6.1) happens to be a cubic equation in the variable C_{lF} . When extraneous branches of the solution are discarded, the final results of this process can be summarized as shown in Table 2.6.2. Note that the single equation (2.6.1) is now replaced by the two expressions (2.6.3) and (2.6.4) which are applicable over different ranges.

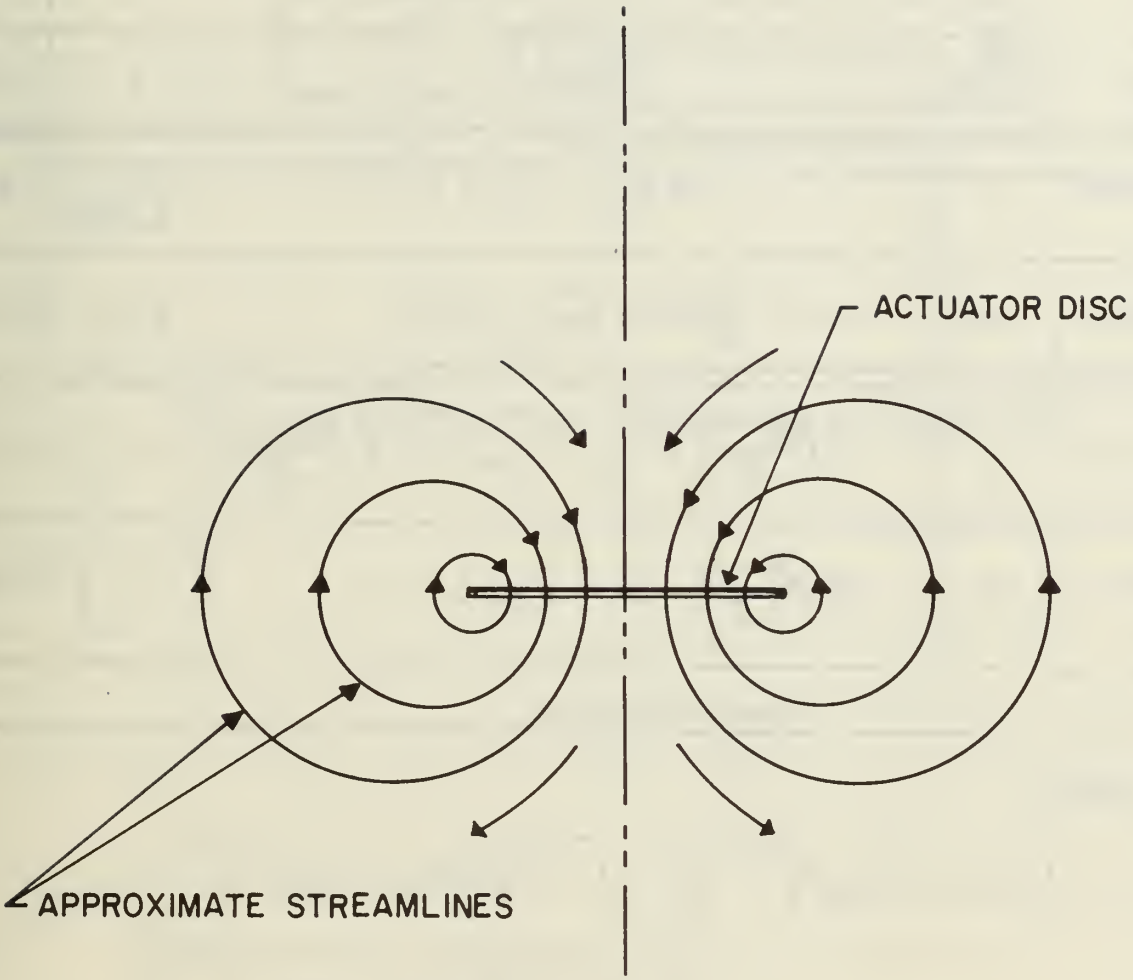

Fig. 2.6.3 SCHEMATIC DIAGRAM OF LIFTING ROTOR IN VORTEX RING STATE.

Table 2.6.2 Basic Actuator Performance Relations

as Functions of Power Coefficient in ρ, D, V System

Mode	Symbol	Range	φ	Eq.
Propulsive	P	$0 \leq (C_{lP} - C_{lPf}) \leq +\infty$	+1	(2.6.3)
Windmill	W	$-\frac{2\pi}{27} \leq (C_{lP} - C_{lPf}) \leq 0$	N.A.	(2.6.4)
Transition	T	$-\frac{\pi}{6}\left(\frac{\sqrt{3}-1}{\sqrt{3}}\right) \leq (C_{lP} - C_{lPf}) \leq +\frac{\pi}{6}\left(\frac{\sqrt{3}+1}{\sqrt{3}}\right)$	N.A.	(2.6.5)
Reverse	R	$+\frac{\pi}{6}\left(\frac{\sqrt{3}+1}{\sqrt{3}}\right) \leq (C_{lP} - C_{lPf}) \leq +\infty$	-1	(2.6.3)

Basic Equations

Modes P and R

$$C_{lF} = \left\{\frac{\pi}{4}(C_{lP} - C_{lPf})^2\right\}^{1/3} \left\{\left[1 + \sqrt{1 + \frac{2\pi\varphi}{27}(C_{lP} - C_{lPf})^{-1}}\right]^{1/3} + \left[1 - \sqrt{1 + \frac{2\pi\varphi}{27}(C_{lP} - C_{lPf})^{-1}}\right]^{1/3}\right\} \quad (2.6.3)$$

Mode W

$$C_{lF} = \sqrt{-\frac{2\pi}{3}(C_{lP} - C_{lPf})}\cos\left[\frac{\alpha}{3} + m\,\frac{2\pi}{3}\right] \quad (2.6.4)$$

where $\cos\alpha = \sqrt{-\frac{27}{2\pi}(C_{lP} - C_{lPf})}$, $0 \leq \alpha \leq \frac{\pi}{2}$, and where m has the values -1 and +1, respectively, over the following sub-ranges:

(Table continues on next page)

Table 2.6.2 Cont'd

m = -1	$-\frac{2\pi}{27} \leq (C_{lP} - C_{lPf}) \leq 0$
m = +1	$-\frac{\pi}{6}\left(\frac{\sqrt{3}-1}{\sqrt{3}}\right) \geq (C_{lP} - C_{lPf}) \geq -\frac{2\pi}{27}$

Mode T

$$C_{lF} = -\frac{\pi}{3\sqrt{3}} - (C_{lP} - C_{lPf}) \qquad (2.6.5)$$

Note: For definitions of coefficients, see Table 2.4.1.

However, the analytical solutions summarized in Tables 2.6.1 and 2.6.2 are entirely equivalent, and both generate precisely the same family of curves, namely, that family previously shown in Fig. 2.6.2.

It should be appreciated that the form of solution based on the ρ, D, V dimensional system as illustrated in Fig. 2.6.2 can be useful in any situation in which V is both known and non-vanishing. The windmill is perhaps the best example, because no windmill can generate useful shaft power, nor even a useful drag force, unless V is non-zero. Conversely, this particular reference system is virtually useless for dealing with any situation in which performance under static conditions, V = 0, is a significant factor because under these conditions all four of the dimensionless coefficients C_{lF}, C_{lP}, C_{lPf} and C_{lN} become infinite and comparatively meaningless. The important cases of the propeller under static thrust or the lifting rotor in stationary hovering flight are examples of situations which cannot be usefully treated within the framework of the ρ, D, V dimensional system. To deal with these problems we must employ the other alternative systems.

2.7 The Basic Solution in the ρ, D, $|P|$ System

In the previous ρ, D, V dimensional system, the parameters ρ and D are innately positive, and V is restricted to non-negative values by definition. We note, however, that in the present dimensional system, shaft power P itself may be either positive or negative, depending on the particular mode of operation considered. It is essential that all dimensional reference quantities be restricted to positive values only, hence we take $|P|$ rather than P as the appropriate reference quantity.

We also note that the overall transition range, mode T, must now be sub-divided into two sub-intervals corresponding, respectively, to positive and negative values of net shaft power P. We denote these as modes TR and TW, respectively.

Upon changing from the ρ, D, V system to the ρ, D, $|P|$ system, the original pair of fundamental equations as previously given in Table 2.6.1 are thereby converted into the corresponding pair of equations now shown in Table 2.7.1. Of course the change involved is purely a matter of algebraic form; the underlying physical relationships are still precisely the same as before.

We observe that Eq. (2.7.1) of the table is linear in C_{2V} but cubic in C_{2F}, whereas Eq. (2.7.2) is linear in C_{2F} but cubic in C_{2V}. Each equation is here solved for the linear term thereby expressing the final relations in their simplest algebraic forms, as shown. However, it is sometimes desirable to write both these relations for C_{2F} in the form of an explicit function of C_{2V}. In this case it becomes useful to distinguish between the power input and power output modes. The solutions for these two cases are summarized separately in Tables 2.7.2 and 2.7.3.

Conversely, it is sometimes convenient to be able to solve all relations consistently for C_{2V} as a function of C_{2F}. This requires the inversion of Eq. (2.7.2) which is summarized in Table 2.7.4.

Table 2.7.1 Basic Actuator Performance Relations

in ρ, D, $|P|$ System

Mode	Symbol	Range	σ	φ	Eq.
Power Input Modes -					
Propulsive	P	$+\left[\frac{\pi}{2}(1-C_{2Pf})^2\right]^{1/3} \geq C_{2F} \geq 0$	+1	+1	(2.7.1
Reverse	R	$-\left[\frac{\pi}{2}(1-C_{2Pf})^2\right]^{1/3} \geq C_{2F} \geq -\left[\frac{\pi}{2}(\sqrt{3}+1)(1-C_{2Pf})^2\right]^{1/3}$	+1	-1	(2.7.1
Transition (Power In)	TR	$+\left[\frac{6}{\pi}\left(\frac{\sqrt{3}}{\sqrt{3}+1}\right)(1-C_{2Pf})\right]^{1/3} \leq C_{2V} \leq +\infty$	+1	N.A.	(2.7.2
Power Output Modes -					
Windmill	W	$0 \geq C_{2F} \geq -\left[\frac{\pi}{2}(\sqrt{3}-1)(1+C_{2Pf})^2\right]^{1/3}$	-1	+1	(2.7.1
Transition (Power Out)	TW	$+\left[\frac{6}{\pi}\left(\frac{\sqrt{3}}{\sqrt{3}-1}\right)(1+C_{2Pf})\right]^{1/3} \leq C_{2V} \leq +\infty$	-1	N.A.	(2.7.2
Basic Equations -					
Modes P, R, W		$C_{2V} = \frac{(1-\sigma C_{2Pf})}{\sigma C_{2F}} - \frac{2\sigma}{\pi\varphi}\frac{C_{2F}^2}{(1-\sigma C_{2Pf})}$			(2.7.1
Modes TR and TW		$C_{2F} = -\frac{\pi}{3\sqrt{3}}C_{2V}^2 - \frac{\sigma(1-\sigma C_{2Pf})}{C_{2V}}$			(2.7.2

Note: For definitions of coefficients, see Table 2.4.1.

Table 2.7.2 Basic Actuator Performance Relations in Terms of Velocity Coefficient for Power Input Modes in ρ, D, |P| System

Mode	Symbol	Range	φ	Eq.
Propulsive	P	$0 \leq C_{2V} \leq +\infty$	+1	(2.7.3)
Reverse	R	$0 \leq C_{2V} \leq +\left[\frac{27}{2\pi}(1 - C_{2Pf})\right]^{1/3}$	-1	(2.7.3)
Transition (Power In)	TR	$\left[\frac{27}{2\pi}(1 - C_{2Pf})\right]^{1/3} \leq C_{2V} \leq +\infty$	N.A.	(2.7.4)

Basic Equations

Modes P and R

$$C_{2F} = \left\{\frac{\pi}{4}(1 - C_{2Pf})^2\right\}^{1/3} \left\{\left[1 + \sqrt{1 + \frac{2\pi\varphi}{27}\frac{C_{2V}^3}{(1 - C_{2Pf})}}\right]^{1/3} + \left[1 - \sqrt{1 + \frac{2\pi\varphi}{27}\frac{C_{2V}^3}{(1 - C_{2Pf})}}\right]^{1/3}\right\} \tag{2.7.3}$$

Mode TR

$$C_{2F} = -\frac{\pi}{3\sqrt{3}} C_{2V}^2 - \frac{(1 - C_{2Pf})}{C_{2V}} \tag{2.7.4}$$

Note: For definitions of coefficients, see Table 2.4.1.

Table 2.7.3 Basic Actuator Performance Relations in Terms of Velocity Coefficient for Power Output Modes in ρ, D, $|P|$ System

Mode	Symbol	Range	Eq.
Windmill	W	$\left[\frac{27}{2\pi}(1 + C_{2Pf})\right]^{1/3} \leq C_{2V} \leq +\infty$	(2.7.5)
Transition (Power Out)	TW	$\left[\frac{6}{\pi}\left(\frac{\sqrt{3}}{\sqrt{3}-1}\right)(1 + C_{2Pf})\right]^{1/3} \leq C_{2V} \leq +\infty$	(2.7.6)

Basic Equations -

Mode W

$$C_{2F} = \sqrt{\frac{2\pi}{3}(1 + C_{2Pf})\, C_{2V}} \cos\left[\frac{\alpha}{3} + m\left(\frac{2\pi}{3}\right)\right] \qquad (2.7.5)$$

where $\cos\alpha = \sqrt{\frac{27}{2\pi}\frac{(1 + C_{2Pf})}{C_{2V}^3}}$, $0 \leq \alpha \leq \frac{\pi}{2}$, and where m has the values -1 and +1, respectively, over the following sub-ranges:

m = -1	$\left[\frac{27}{2\pi}(1+C_{2Pf})\right]^{1/3} \leq C_{2V} \leq +\infty$
m = +1	$\left[\frac{27}{2\pi}(1+C_{2Pf})\right]^{1/3} \leq C_{2V} \leq \left[\frac{6}{\pi}\left(\frac{\sqrt{3}}{\sqrt{3}-1}\right)(1+C_{2Pf})\right]^{1/3}$

Mode TW

$$C_{2F} = -\frac{\pi}{3\sqrt{3}} C_{2V}^2 + \frac{(1 + C_{2Pf})}{C_{2V}} \qquad (2.7.6)$$

Note: For definitions of coefficients, see Table 2.4.1.

Table 2.7.4 Basic Actuator Performance Relation in Terms of Force Coefficient for Transition Modes in ρ, D, $|P|$ System

Mode	Symbol	Range	α	Eq.
Transition (Power In)	TR	$-\left[\frac{\pi}{2}(\sqrt{3}+1)(1-C_{2Pf})^2\right]^{1/3} \geq C_{2F} \geq -\infty$	+1	(2.7.7)
Transition (Power Out)	TW	$-\left[\frac{\pi}{2}(\sqrt{3}-1)(1+C_{2Pf})^2\right]^{1/3} \geq C_{2F} \geq -\infty$	-1	(2.7.7)

Basic Equation -

Modes TR and TW

$$C_{2V} = 2\sqrt{\frac{\sqrt{3}}{\pi}(-C_{2F})}\cos\frac{\beta}{3} \qquad (2.7.7)$$

where

$$\cos\beta = -\frac{3}{2}\sqrt{\frac{\pi}{\sqrt{3}}}\frac{\sigma(1-\sigma C_{2Pf})}{(-C_{2F})^{3/2}}$$

Note: For definition of coefficients, see Table 2.4.1.

The form of the solution is shown graphically in Fig 2.7.1 for the power input modes and in Fig 2.7.2 for the power output modes. In each case the solution consists of a family of curves of C_{2F} versus C_{2V} with the power loss coefficient C_{2Pf} as parameter. Of course the curves for $C_{2Pf} = 0$ once again represent a limit that any real actuator may approach but never exceed.

The upper part of Fig. 2.7.1 represents a propeller in normal operation. The lower part represents a propeller under conditions of power-on reversed thrust. Fig. 2.7.1 represents a windmill generating useful power and undergoing a drag force. We can think of this case as depicting a windmill of fixed size generating fixed shaft power under various wind velocities. Note the existence of a limiting velocity below which the specified power cannot be attained. This corresponds to the critical value $C_{2V}\Big)_{cr} = \left[\frac{27}{2\pi}(1 + C_{2Pf})^2\right]^{1/3}$. Also at any given value of C_{2V} above the critical, there are of course two solutions corresponding to low and high drag, respectively.

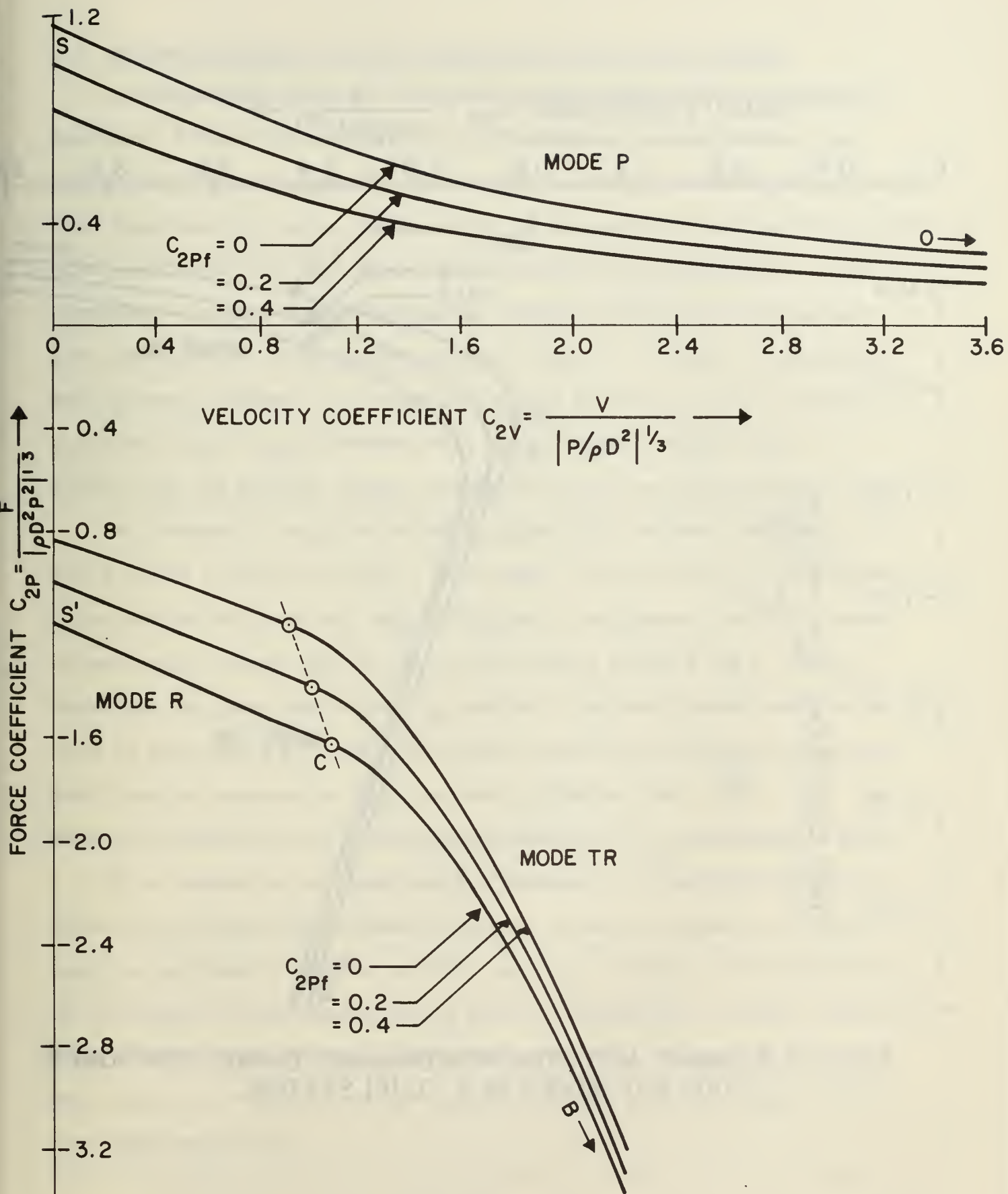

Fig. 2.7.1 BASIC ACTUATOR PERFORMANCE CURVES FOR POWER INPUT MODES IN ρ, D, |P| SYSTEM.

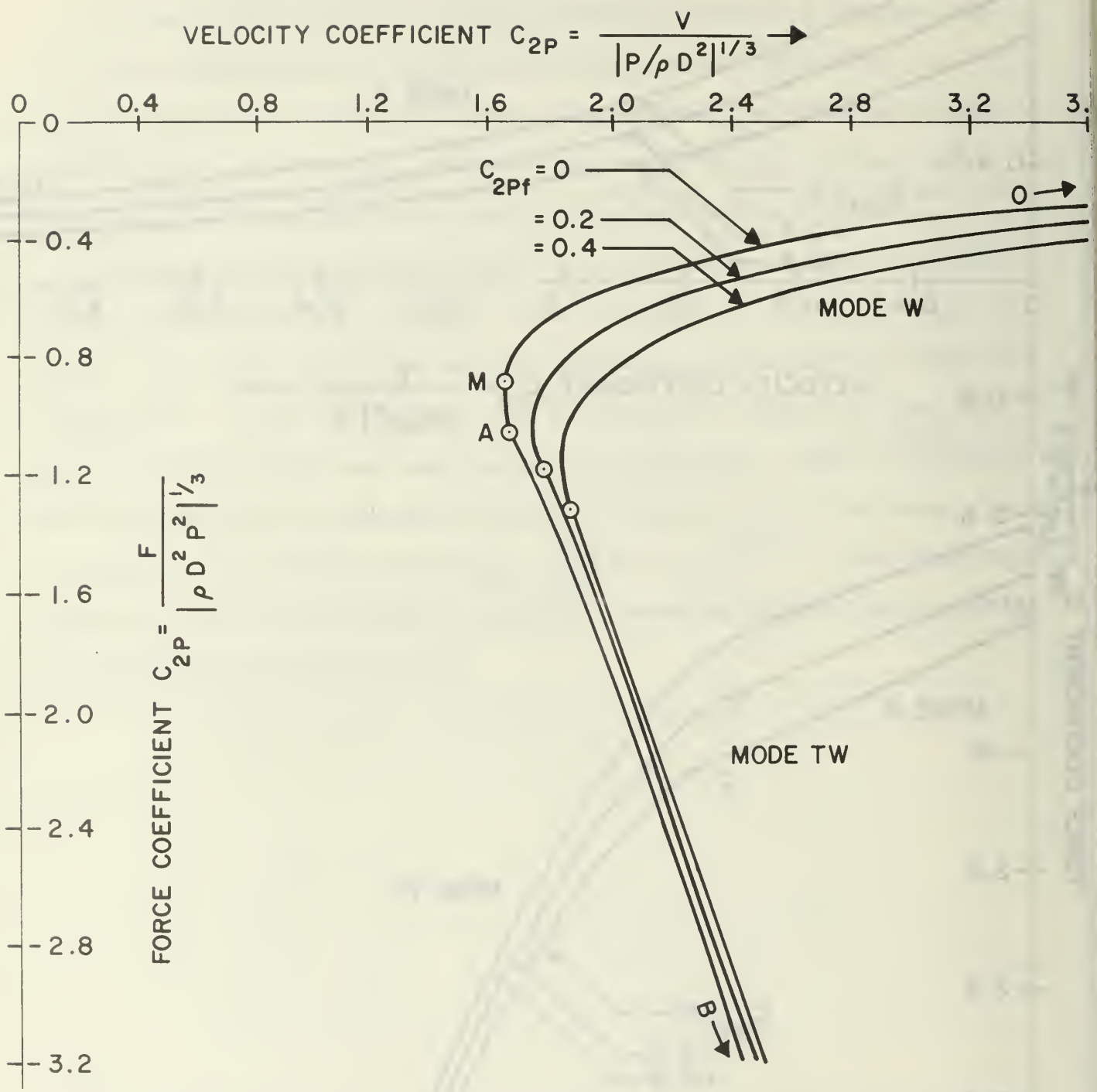

Fig. 2.7.2 BASIC ACTUATOR PERFORMANCE CURVES FOR POWER OUT PUT MODES IN ρ, D, |P| SYSTEM.

2.8 The Basic Solution for the Lifting Rotor in the ρ, D, L System

Straightforward algebraic conversion of the original pair of fundamental equations of Table 2.6.1 into the ρ, D, L dimensional system produces the corresponding pair of equations for the lifting rotor as shown in Table 2.8.1. These equations show power coefficient C_{3P} as an explicite function of rate of climb coefficient $C_{3\dot{H}}$, with power loss coefficient C_{3Pf} as parameter. This arrangement not only yields the simplest algebraic result, but is also the most convenient for various other purposes as well. Of course, if necessary, both of these relations can be readily inverted to give $C_{3\dot{H}}$ as an explicit function of $(C_{3P} - C_{3Pf})$; however, this again entails solving a cubic equation and the detailed results obtainable in this way are not included here.

The fundamental relation defined in Table 2.8.1 is shown graphically in Fig. 2.8.1 as a family of curves. Once again, the curve for $C_{3Pf} = 0$ represents a performance limit that any real lifting rotor can approach but never exceed. Of particular interest are the two critical points marked S and B. Point S shows that the power coefficient C_{3P} required to maintain steady hovering can never be less than $\sqrt{\frac{2}{\pi}} = 0.798$. Point B shows that the rate of descent at zero net shaft power as measured by $|C_{3\dot{H}}|$ can never be smaller than $\sqrt{\frac{3\sqrt{3}}{\pi}} = 1.286$. The changes of these values with increasing loss coefficient C_{3Pf} is also plainly shown.

It is noteworthy that these results represent an elementary solution in closed form over the entire operating range! Hitherto, elementary solutions based on the ordinary momentum analysis have been available over those portions of the range which correspond, in the present terminology, to modes P and W only. Moreover, the present results embody the useful parameter C_{3Pf} which facilitates the comparison of any real lifting rotor with the ideal, or with some other real rotor.

Table 2.8.1 Basic Lifting Rotor Performance Relations in Terms of Rate of Climb Coefficient in ρ, D, L System

Mode	Symbol	Range	φ	τ	σ_i	Eq.
Propulsive	P	$+\infty \geq C_{3\dot{H}} \geq 0$	+1	+1	+1	(2.8.1
Reverse	R	$0 \geq C_{3\dot{H}} \geq -\left\{\frac{\pi}{6}(\sqrt{3}+1)\right\}^{-\frac{1}{2}}$	-1	-1	+1	(2.8.1
Transition	T	$-\left\{\frac{\pi}{6}(\sqrt{3}+1)\right\}^{-\frac{1}{2}} \geq C_{3\dot{H}} \geq -\left\{\frac{\pi}{6}(\sqrt{3}-1)\right\}^{-\frac{1}{2}}$	N.A.	N.A.	N.A.	(2.8.2
Windmill	W	$-\left\{\frac{\pi}{6}(\sqrt{3}-1)\right\}^{-\frac{1}{2}} \geq C_{3\dot{H}} \geq -\infty$	+1	-1	-1	(2.8.1

Basic Equations -

Modes P, R, W

$$C_{3P} = \frac{C_{3\dot{H}}}{2} + \tau_i \sqrt{\left(\frac{C_{3\dot{H}}}{2}\right)^2 + \left(\frac{2\tau}{\pi\varphi}\right)} + C_{3Pf} \qquad (2.8.1$$

Mode T

$$C_{3P} = +\frac{\pi}{3\sqrt{3}} C_{3\dot{H}}^{\,3} - C_{3\dot{H}} + C_{3Pf} \qquad (2.8.2$$

Note 1: At $C_{3\dot{H}} = 0$, Eq. (2.8.1) gives $C_{3P} = \sqrt{\frac{2}{\pi}} + C_{3Pf}$.

Note 2: At $C_{3P} = 0$, Eq. (2.8.2) gives $C_{3\dot{H}} = \sqrt{\frac{4\sqrt{3}}{\pi}} \cos\left(\frac{\delta}{3} + \frac{2\pi}{3}\right)$

where $\cos\delta = -\sqrt{\frac{9\pi}{4\sqrt{3}}} C_{3Pf}$, $\frac{\pi}{2} \leq \delta \leq \pi$. In the limit $C_{3Pf} = 0$, this reduces to $C_{3\dot{H}} = -\sqrt{\frac{3\sqrt{3}}{\pi}}$.

Note 3: For definitions of coefficients, see Table 2.4.1.

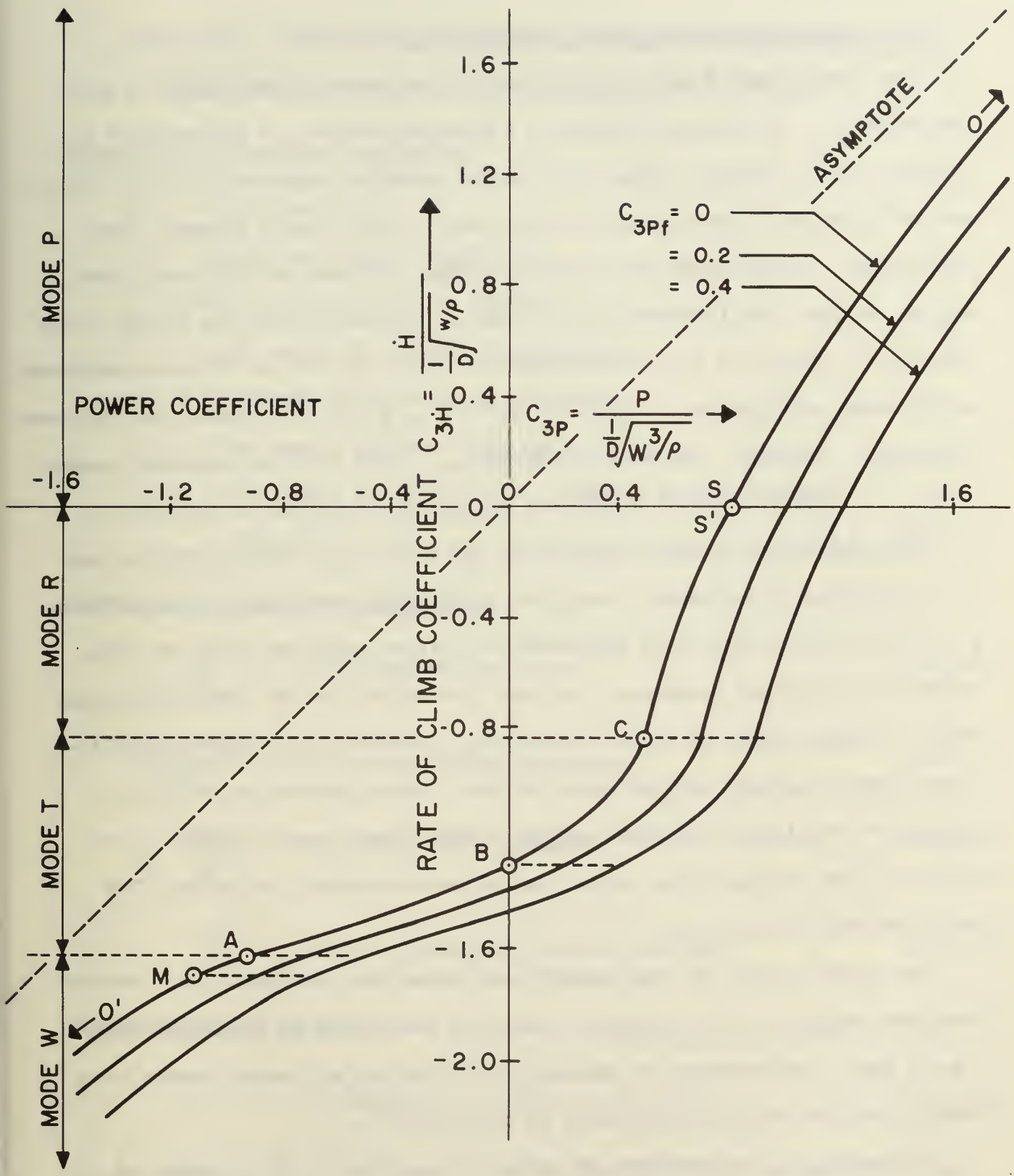

Fig. 2.8.1 BASIC ACTUATOR PERFORMANCE CURVES FOR LIFTING ROTOR IN ρ, D, L SYSTEM.

2.9 The Idealized Rotating Finite Torque Actuator

The ideal actuator mainly considered in this paper is essentially a zero torque device. In section 9, however, a detailed analysis is presented of an actuator which, although ideal in all other respects, operates at finite torque and at finite shaft speed. Such a device will always operate somewhat less effectively than the ideal zero torque actuator, although at high shaft speed and low torque, the difference will be small. In dealing with the finite torque actuator, it turns out to be advantageous to revert to the use of the conventional performance coefficients C_F, C_P and J based on ρ, N and D as dimensional reference parameters. Moreover, the relations among C_F, C_P and J can be expressed parametrically in terms of certain slipstream parameters as defined in Table 2.9.1.

The analysis of section 9 shows that the torque and rotation effects lead to the creation of peripheral velocities in the slipstream leaving the actuator. A solution is found for these peripheral velocities which maintains the axial velocity distribution unchanged from what it would be for the ideal zero torque case. In other words the axial velocities at the disc and in the remote slipstream remain constant and uniform as before. The slipstream is found to consist of two distinct regions, namely, a small inner core of radius r_0 in which the flow remains purely axial, and an outer annulus in which the flow is of the free vortex type.

The chief results of this analysis are summarized in Table 2.9.1. Notice that this analysis of the rotating actuator is restricted to the simple modes P and W only; the extension of the analysis to include all modes appears to be feasible but has not been undertaken in this paper.

In principle, the equations of Table 2.9.1 suffice to fix a family of curves of C_F versus J, with C_P as the parameter whose value changes from one

Table 2.9.1 Conventional Performance Coefficients of Idealized Finite Torque Actuator in Terms of Slipstream Parameters

Dimensional Slipstream Parameters

R = Slipstream radius

r = Slipstream radial co-ordinate

ω = Shaft angular velocity (rad/sec)

V = Axial velocity of undisturbed flow

V_S = Slipstream axial velocity (constant)

V_u = Slipstream peripheral velocity

$V_u r = \Gamma$ Slipstream vortex strength (Constant over the region $r_0 \leq r \leq R$.) (2.9.1)

Dimensionless Slipstream Parameters

$$\frac{V}{\omega R} = \mu \quad \text{Slipstream advance ratio} \tag{2.9.2}$$

$$\frac{(V_S - V)}{\omega R} = \Lambda \quad \text{Slipstream loading parameter} \tag{2.9.3}$$

$$\frac{\Gamma}{\omega R^2} = \gamma \quad \text{Slipstream swirl parameter} \tag{2.9.4}$$

$$\frac{r_0}{R} = \eta_0 \quad \text{Relative radius of non-swirling core} \tag{2.9.5}$$

Range of Loading Parameter

$$-2\left(\frac{\sqrt{3}-1}{\sqrt{3}}\right)\mu \leq \Lambda \leq +\left(\sqrt{1+\mu^2} - \mu\right) \tag{2.9.6}$$

Positive values of Λ correspond to mode P, negative values to mode W. Other modes are not considered in this particular analysis.

(Table continues on next page)

Auxiliary Functions

$$\zeta = \left\{ \frac{1 - \sqrt{1 - 2\left(\mu + \frac{\Lambda}{2}\right)\Lambda}}{\left(\mu + \frac{\Lambda}{2}\right)\Lambda} \right\} \tag{2.9.7}$$

$$= 1 + \tfrac{1}{2}\left(\mu + \tfrac{\Lambda}{2}\right)\Lambda + \tfrac{1}{2}\left(\mu + \tfrac{\Lambda}{2}\right)^2 \Lambda^2 + \text{----}$$

$$\gamma = \zeta\left(\mu + \frac{\Lambda}{2}\right)\Lambda \tag{2.9.8}$$

$$\frac{1}{\eta_0^2} = 1 + \frac{2}{\zeta\gamma} \tag{2.9.9}$$

Parametric Solutions for Conventional Performance Coefficients

$$C_F = \frac{\pi^3}{4}\left(\frac{\mu + \frac{\Lambda}{2}}{\mu + \Lambda}\right)^2 \left\{ (\mu + \Lambda)\Lambda\left(1 - \eta_0^2\right) - \frac{\gamma^2}{2}\left[\ln\frac{1}{\eta_0^2} - \left(1 - \eta_0^2\right)\right] + \tfrac{1}{2}\Lambda^2\eta_0^2 \right\} \tag{2.9.10}$$

$$C_P = \frac{\pi^4}{4}\left(\frac{\mu + \frac{\Lambda}{2}}{\mu + \Lambda}\right)^{5/2} (\mu + \Lambda)\gamma\left(1 - \eta_0^2\right) \tag{2.9.11}$$

$$J = \pi\mu\sqrt{\frac{\mu + \frac{\Lambda}{2}}{\mu + \Lambda}} \tag{2.9.12}$$

Static Conditions and Maximum Loading Limits

Under static conditions (V = 0), the above relations simplify as indicated in section 9.13, with results as shown in Fig. 2.9.1.

Under maximum loading conditions, they simplify as indicated in section 9.14, with results as shown in Fig. 2.9.2.

(End of Table 2.9.1)

curve to the next. The calculations required for this purpose are straightforward but tedious. At the time of writing, they still remain to be carried out. When completed, the resulting family of curves will define idealized performance limits which provide a suitable standard of comparison for the performance of any real single rotation actuator. By application of the rationale explained more fully in section 9, these results may also be used to evaluate the idealized rotation power loss P_N for any prescribed operating condition.

Under static conditions ($V = 0$), the general solution summarized in Table 2.9.1 reduces to the special form given in section 9.13. The corresponding result is shown in Fig. 2.9.1 of this section in the form of a curve of the quanties C_F and $C_F/C_P^{2/3}$ plotted versus C_P. The intercept at $C_P = 0$ corresponds to the limiting performance at zero torque, and the drop-off of this relative thrust parameter with increasing power coefficient C_P shows the effect of rotation losses.

Another special case of theoretical interest is that corresponding to the maximum loading theoretically attainable, as analyzed in section 9.14. The essential results are summarized here in Fig. 2.9.2 which shows $C_F)_{MAX}$ and $C_P)_{MAX}$ plotted as functions of J. Note that this absolute performance limit is deduced purely from fundamental dynamical principles and without any reference whatever to any empirical data or to such complex and highly variable details of the flow field as local lift coefficients, separation effects or the like! These latter effects can and do reduce the performance of any actual device well <u>below</u> the limits shown in Fig. 2.9.2. The essential point, however, is that there is no feasible way to raise the actual performance <u>above</u> these limits.

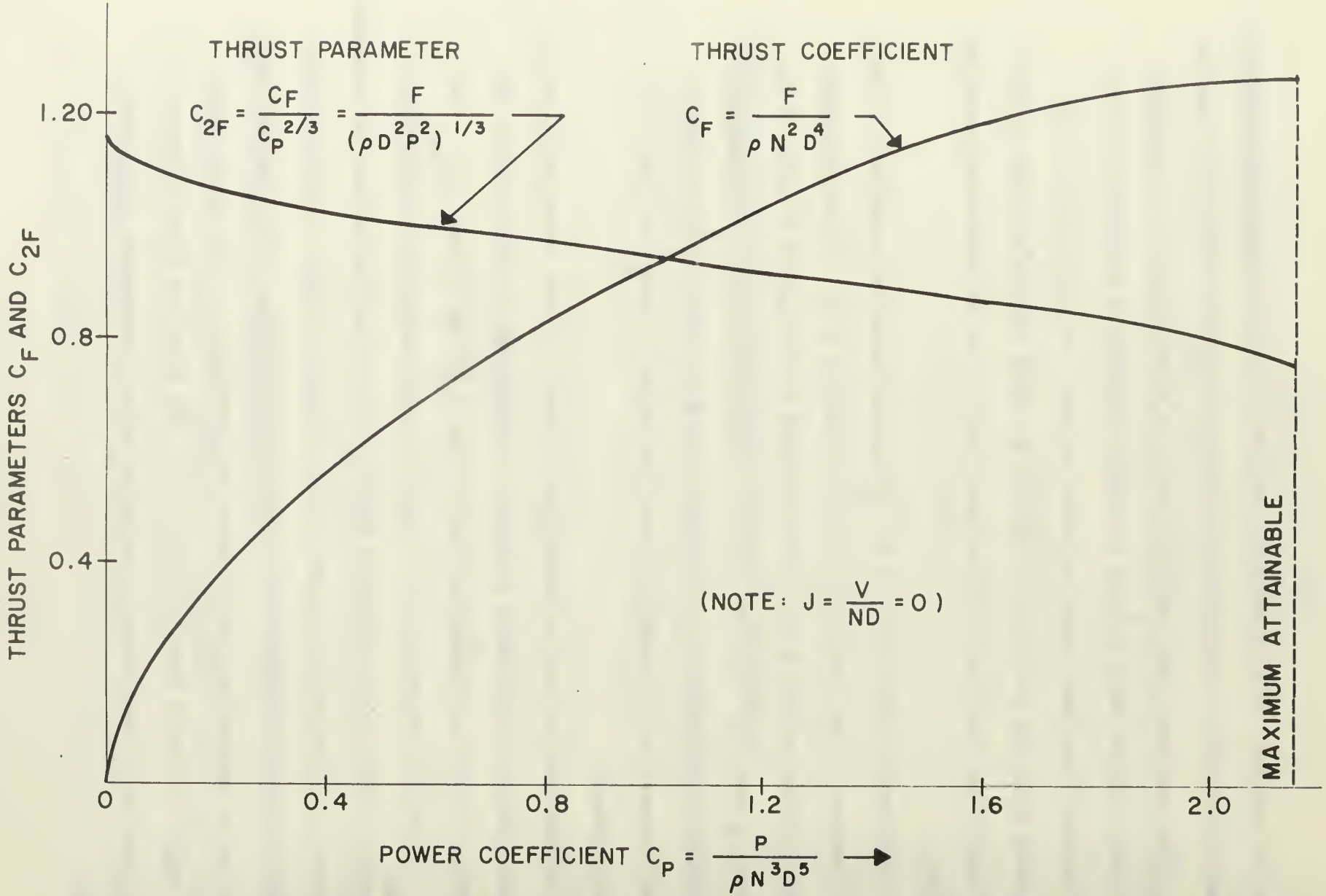

Fig. 2.9.1 STATIC THRUST PARAMETERS VERSUS POWER COEFFICIENT FOR IDEAL FINITE TORQUE ACTUATOR.

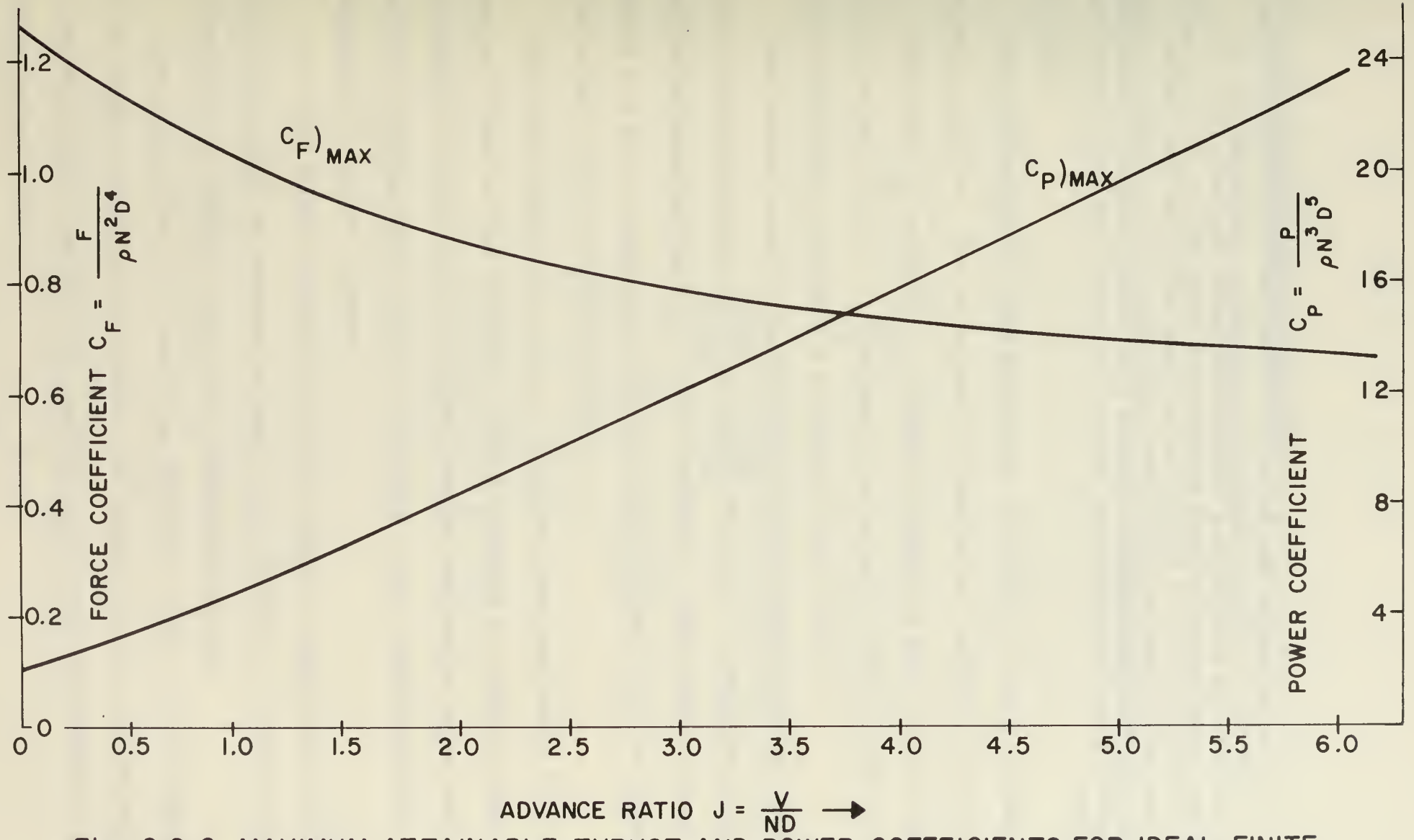

Fig. 2.9.2 MAXIMUM ATTAINABLE THRUST AND POWER COEFFICIENTS FOR IDEAL FINITE TORQUE ACTUATOR.

It is also noteworthy that Table 2.9.1 summarizes the performance of the ideal finite torque actuator in a comparatively simple algebraic form. In general these results yield information that goes well beyond what can be deduced from the usual elementary analysis which simply neglects rotation effects altogether.

2.10 Stability of the Ideal Lifting Rotor

In this subsection, we summarize the dynamic response of an ideal lifting rotor ($P_f = 0$) to small perturbations from equilibrium during vertical ascent or descent. At the equilibrium state, lift L is equal to the rotor craft weight W, but lift is subject to small perturbations δL about the equilibrium value.

It is advantageous in this application to choose ρ, D and W as dimensional reference parameters. The corresponding dimensionless coefficients of power C_{3P}, climb rate $C_{3\dot{H}}$, and lift C_{3L} are then as defined in Eqs. (2.10.1) through (2.10.3) of Table 2.10.1. It also simplifies matters to express time in terms of the dimensionless coordinate θ as defined in Eq. (2.10.4).

The inherent stability characteristics of the lifting rotor are expressed by the partial derivatives $\left(\frac{\partial C_{3P}}{\partial C_{3\dot{H}}}\right)$ and $\left(\frac{\partial C_{3P}}{\partial C_{3L}}\right)$ which must be evaluated along the equilibrium operating line $C_{3L} = 1$. For simplicity, these derivatives are denoted as X and Y, respectively, and are known functions of $C_{3\dot{H}}$, as summarized in Eqs. (2.10.5) through (2.10.8).

The power input to the rotor or, in descent, the power output from the rotor may either be held constant, or may be modulated by a control system in response to sensed values of the perturbation acceleration and/or perturbation velocity, according to Eq. (2.10.9). Constants μ and ν express these two components of the power response.

The final dynamic response of the rotor craft to a small perturbation is then exponential in character as shown in Eq. (2.10.10). A stable response corresponds to a negative value of the exponential factor β.

The solution for β is given by Eq. (2.10.11). This is seen to depend on the functions X and Y which describe the inherent stability characteristics of the rotor itself, and upon the constants μ and ν which characterize the power control system, if any.

Table 2.10.1 Stability of Idealized Lifting Rotor

in Vertical Ascent or Descent

($P_f = 0$)

Dimensionless Coefficients

$$C_{3P} = \frac{P}{\frac{1}{D}\sqrt{\frac{W^3}{\rho}}} \quad (2.10.1) \qquad C_{3L} = \frac{L}{W} \quad (2.10.3)$$

$$C_{3\dot{H}} = \frac{\dot{H}}{\frac{1}{D}\sqrt{\frac{W}{\rho}}} \quad (2.10.2) \qquad \theta = \frac{t}{\frac{1}{gD}\sqrt{\frac{W}{\rho}}} \quad (2.10.4)$$

Actuator Derivatives at Equilibrium ($C_{3L} = 1$)

Modes P, W and R

$$X = \frac{\partial C_{3P}}{\partial C_{3\dot{H}}} = \tfrac{1}{2} + \frac{\frac{C_{\dot{H}}}{4}}{\sigma_i \sqrt{\left(\frac{C_{\dot{H}}}{2}\right)^2 + \frac{2\tau}{\pi\varphi}}} \quad (2.10.5)$$

$$Y = \frac{\partial C_{3P}}{\partial C_L} = \frac{C_{\dot{H}}}{2} + \frac{\left[\left(\frac{C_{\dot{H}}}{2}\right)^2 + \frac{3}{\pi}\frac{\tau}{\varphi}\right]}{\sigma_i \sqrt{\left(\frac{C_{\dot{H}}}{2}\right)^2 + \frac{2}{\pi}\frac{\tau}{\varphi}}} \quad (2.10.6)$$

Mode T

$$X = \frac{\partial C_{3P}}{\partial C_{3\dot{H}}} = -\frac{\pi}{\sqrt{3}}\tau C_{\dot{H}}^2 - 1 \quad (2.10.7)$$

$$Y = \frac{\partial C_{3P}}{\partial C_{3L}} = -C_{\dot{H}} \quad (2.10.8)$$

(Table continues on next page)

Control System Coefficients

$$\delta C_{3P} = - \mu \frac{d}{d\theta} \left[\delta C_{3\dot{H}} \right] - \nu \left[\delta C_{3\dot{H}} \right] \qquad (2.10.9)$$

μ = perturbation acceleration response constant (if any) ≥ 0

ν = perturbation velocity response constant (if any) ≥ 0

Dynamic Response to a Perturbation

$$\left[\delta C_{3\dot{H}} \right] = \left[\delta C_{3\dot{H}} \right]_0 e^{\beta \theta} \qquad (2.10.10)$$

where

$$\beta = - \left\{ \frac{X + \nu}{Y + \mu} \right\} \qquad (2.10.11)$$

Algebraic Signs of Actuator Derivatives

$$X > 0 \quad \text{for all values of } C_{3\dot{H}} \qquad (2.10.12)$$

$$\left.\begin{aligned} Y > 0 \quad & \text{if } C_{3\dot{H}} > - \frac{3}{\sqrt{\pi}} \\ Y < 0 \quad & \text{if } C_{3\dot{H}} < - \frac{3}{\sqrt{\pi}} \end{aligned}\right\} \qquad (2.10.13)$$

Stability

Range of stable response for $\mu = \nu = 0$

$$\beta < 0 \quad \text{for} \quad - \frac{3}{\sqrt{\pi}} < C_{3\dot{H}} < + \infty \qquad (2.10.14)$$

Stability Augmentation -

1. Increasing μ increase stable range
2. Increasing ν -
   a) does not affect stable range
   b) increases response rate (whether stable or unstable)

(End of Table)

Calculations reveal that the rotor derivatives X and Y are as shown in Fig. 2.10.1. This leads to the conclusion that with $\mu = \nu = 0$, the system is inherently stable over the range shown in Eq. (2.10.14). Inspection of Eq. (2.10.11) then shows that the range of stable operation can be extended at will by increasing the acceleration control constant μ. Increasing the velocity control constant ν does not affect the stability range itself, but augments the response rate, whether stable or unstable.

The exponential response rate β which fixes the degree of stability or instability is plotted versus climb rate $C_{\dot{3H}}$ for several cases of interest in Fig. 2.10.2.

It is to be expected that the stability characteristics of any real lifting rotor will generally be considerably less favorable than the stability of the ideal rotor as summarized here.

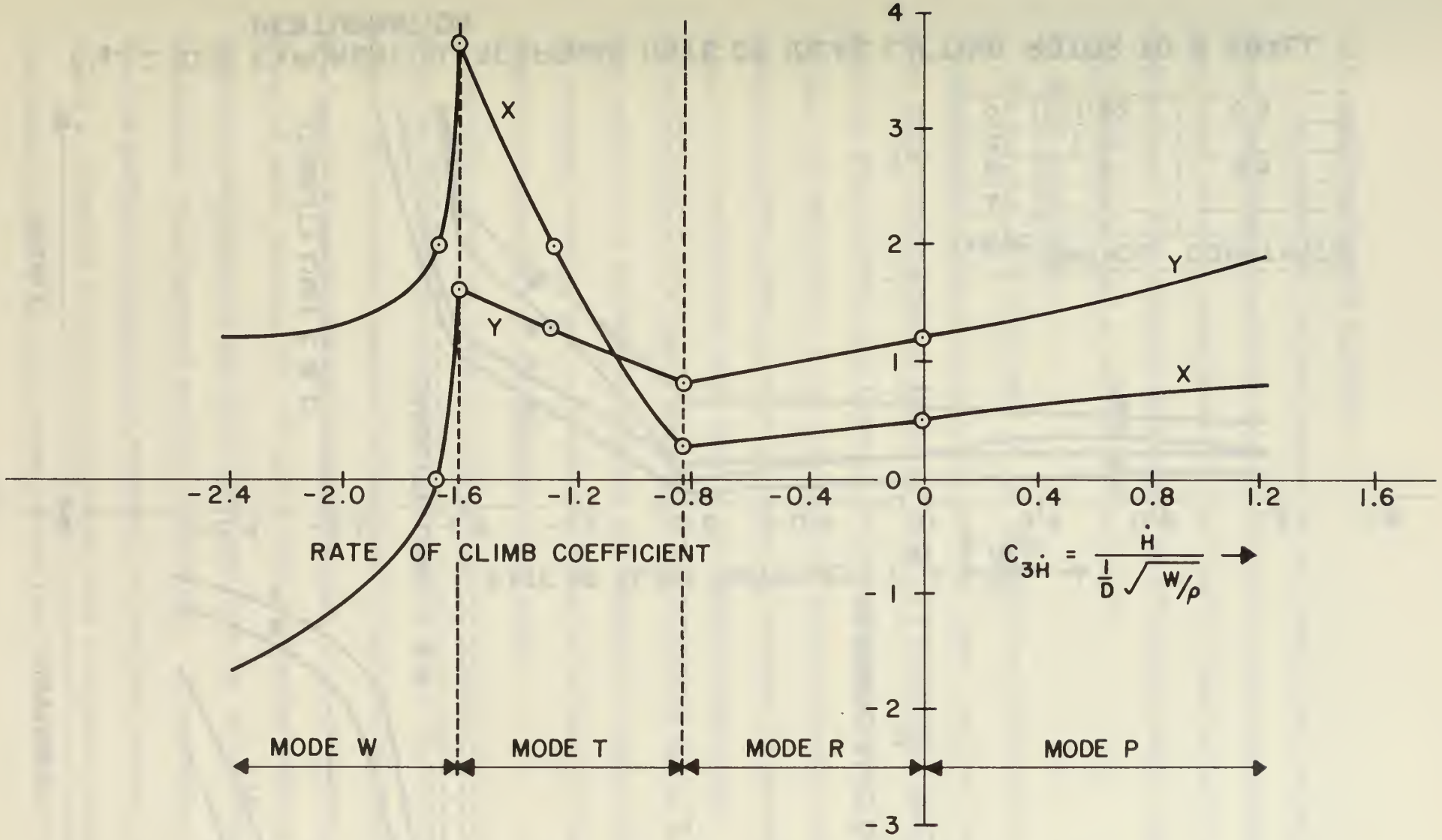

Fig. 2.10.1 STABILITY DERIVATIVES X AND Y FOR IDEAL LIFTING ROTOR.

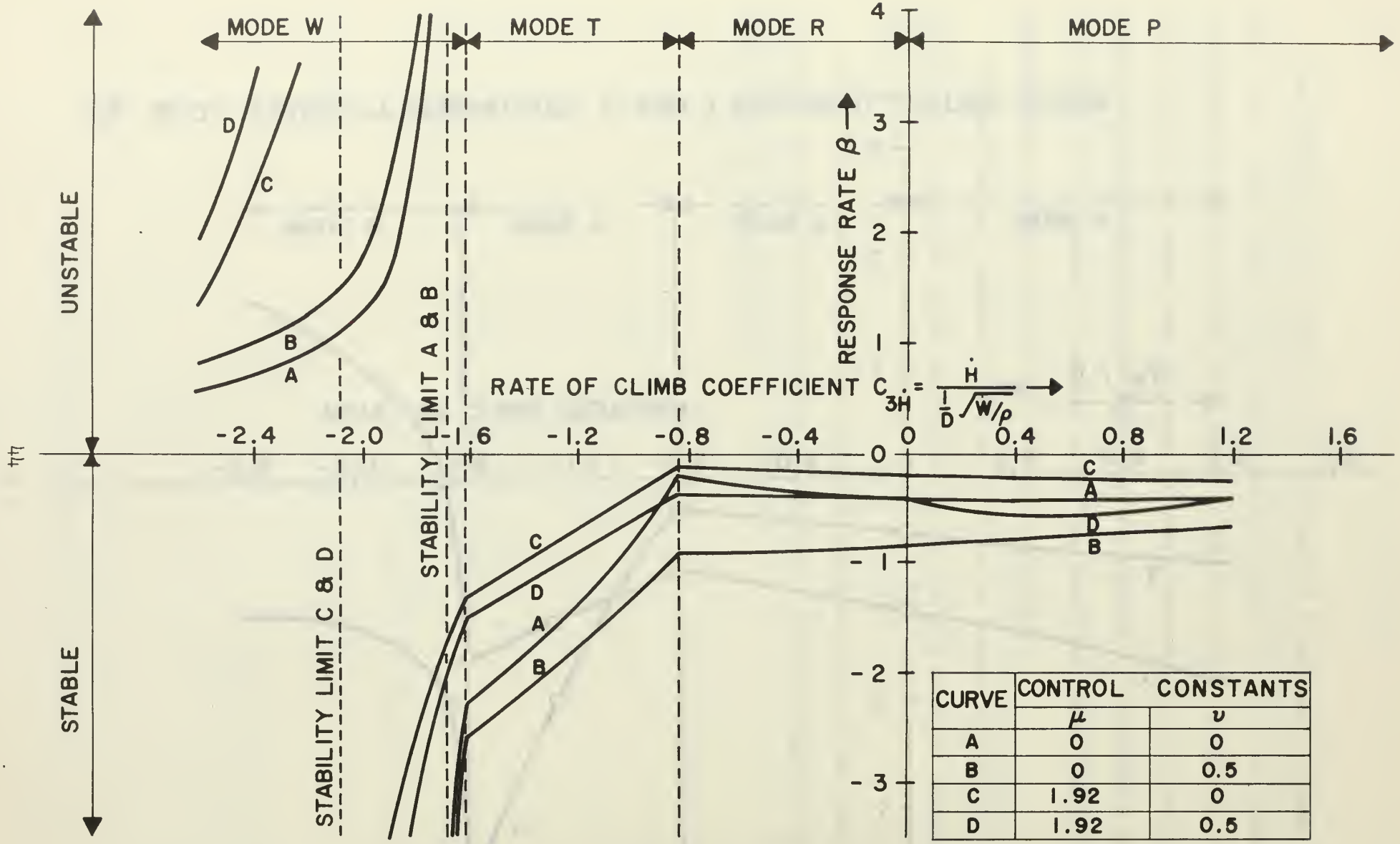

CURVE	CONTROL CONSTANTS	
	μ	ν
A	0	0
B	0	0.5
C	1.92	0
D	1.92	0.5

Fig. 2.10.2 EXPONENTIAL RESPONSE RATE OF IDEAL LIFTING ROTOR TO A SMALL PERTURBATION.

2.11 Auxiliary Figures of Merit

The purpose of this brief subsection is simply to call attention to a number of auxiliary quantities which do not occur in the main theoretical development but which nevertheless provide useful figures of merit in certain applications. These include the concepts of efficiency, power effectiveness and force effectiveness as defined in section 11.

3. Basic Assumptions

The purpose of this analysis is not to predict as accurately as possible the performance of any particular real actuator under specified conditions. It is rather to establish as simple as possible a theoretical performance limit which any real actuator might approach but which none could ever exceed. In general, the performance of any actual device involves physical mechanisms so complex that their effects cannot be adequately assessed by theoretical methods alone; it is necessary to refer also to the results of experiment. Fortunately, the determination of a simple performance limit is a much easier task. For this purpose it is not only permissible but mandatory to neglect all complex but secondary effects, and to concentrate attention exclusively upon the irreducible essentials of the phenemena under study.

For this reason we treat the fluid as incompressible and inviscid, we treat the flow field as possessing polar symmetry about the axis and as being steady, and we neglect possible hydrodynamic instability and turbulence effects. As a result of passing through the actuator, the fluid ultimately undergoes a change of axial velocity ΔV. We assume that this change develops asymptotically within the slipstream as the fluid moves away from the actuator and that, once established, the slipstream persists indefinitely. In particular, for any of the flow patterns involving flow reversal, or involving co-axial streams moving at different velocities and possibly even in opposite senses, we assume that these reversed or co-axial streams persist indefinitely without breaking down.

For any real actuator operating in a real fluid, of course, the slip stream eventually disappears owing to the effects of hydrodynamic instabilities, turbulence and viscous dissipation. These effects are particular important for cases involving flow reversal or co-axial streams, especially if the streams move in opposite senses. Nevertheless, even for real flows, it is usually possible to locate upstream and downstream cross-sections which are sufficiently close to the actuator that the slipstream is still well defined and yet far enough away from the actuator that the pressure in the stream is substantially equal to ambient pressure. For all practical purposes, conditions at such cross-sections are comparable to conditions "at infinity" in the idealized flow pattern. Hence the neglect of slipstream dissipation effects is not as drastic an idealization as it might seem at first glance. Moreover, the usefulness of this approach has long been established in connection with the simple modes P and W. In this paper we are extending the same method to the other modes R and T. Admittedly, these latter modes, especially mode T, are more complex; nevertheless, for the special purpose of establishing a simple performance limit, the method appears to be fully justified.

The idealized analysis also assumes that the velocities are purely axial at all reference cross-sections. Of course, any real propeller or other rotating actuator always exerts some torque upon the fluid and therefore sets up corresponding peripheral velocity components in the slipstream. Creation of the kinetic energy associated with these components absorbs shaft power. The resulting reduction of pressure over much of the slipstream also adversely affects the net thrust. Hence the peripheral velocity components degrade performance and are therefore eliminated from the idealized model, except of course in section 9 where this matter is considered in detail.

Similarly, a real propeller or non-optimal actuator may create non-uniform axial velocities in the far slipstream. Thrust is proportional to the mean axial velocity. Power required is proportional to the mean square of the axial velocity. Clearly, the ratio of useful thrust delivered to power required will be a maximum only if the axial velocity is uniform across the slipstream. Consequently, the analysis of the idealized actuator assumes uniform axial velocities across the far slipstream and across all reference stations. Pressures are also taken as uniform across these stations.

In the transition mode T which involves two oppositely moving co-axial streams, the velocities and pressures are taken as uniform across each stream separately at each station; however, the values of velocity and pressure may in general be different for the two separate streams at a given cross-section.

In the classical momentum analysis of the simple modes P and W, it is assumed implicitly that the net axial force between the fluid which passes through the actuator and the ambient flow is zero or at least that it is negligible compared with the axial force exerted at the actuator disc itself. The corresponding assumption is here extended to modes R and T. In other words, the net axial force between any two co-axial streams is assumed to be negligible in comparison with the axial force exerted on either stream at the actuator disc itself. The only exception to this occurs in section 9 which deals with the finite torque actuator; in this case it is necessary to admit a net axial force across the interface between the nonrotating core and the free vortex flow region.

4. Additional Nomenclature for Main Text

All symbols used in section 2 have previously been defined in subsection 2.1. All other symbols occurring in this paper and not previously defined in subsection

2.1 are summarized below. Again the definitions are arranged according to the section and in the approximate order in which they are introduced in the text.

Section 3

$\Delta V = (V_S - V)$ = net overall increase in axial velocity occurring across the actuator, positive if in the same sense as the velocity V of the undisturbed fluid. ft/sec

Note: For the important special case of static thrust defined by the condition $V = 0$, the velocities V_d, V_S and ΔV, and the force F exerted by the actuator upon the fluid are all in the same sense and all have the same sign which is normally taken as positive.

Section 5

0, u, d, s = symbols or subscripts denoting the following locations, respectively: far upstream side of actuator disc, downstream side of actuator disc, and slipstream far downstream of actuator.

V, V_u, V_d, V_S = respective axial velocities at the above locations, with $V_u = V_d$. ft/sec

p, p_u, p_d, p_S = respective pressures at the above locations, with $p_S = p$. lbf/ft^2

E = total energy per unit mass of fluid upstream of actuator. ft lbf/slug

ΔE = change in total energy per unit mass of fluid produced by actuator. ft lbf/slug

$\dot{m}$ = mass flow rate through actuator disc. slugs/sec

P_S = power lost to slipstream by ideal zero torque actuator. ft lbf/sec

Section 6

C_{lPi} = ideal power coefficient in ρ, D, V system. --

$\lambda = \frac{\Delta V}{V}$ = velocity change ratio. --

U = symbol designating that branch of the formal solution which represents physically unstable operation.

S, O, M, N, U, V, A, B, C, S' = symbols designating significant points on ideal operating envelope as shown in Fig. 6.2.

Section 7

x = fraction of actuator disc area operating in the windmill mode during operation in the transition range. --

$S = \left(\frac{dC_{lPi}}{dC_{lF}}\right)$ = slope of ideal operating curve

A, C = subscripts referring to operation in windmill and reversed modes, respectively, at points A and C of envelope.

Section 8

V_ω = ultimate axial velocity of propagation of vorticity generated at actuator disc. ft/sec

Section 9

Subsection 9.2

P_i' = shaft power of ideal finite torque actuator. ft lbf/sec

P_N = idealized rotation power loss, always non-negative. ft lbf/sec

P_r = residual power loss, always non-negative. ft lbf/sec

Subsection 9.4

p = pressure at edge of slipstream at radius R (equal to pressure of undisturbed flow). lbf/ft^2

p_S = pressure within slipstream at radius $r < R$ (lower than pressure of undisturbed flow). lbf/ft^2

V_u = peripheral velocity in slipstream. ft/sec

Subsection 9.5

p_{SO} = pressure in central non-swirling core region of slipstream. lbf/ft^2

$\eta = \frac{r}{R}$ = slipstream relative radius. --

Subsection 9.10

Λ_{MAX}, ζ_{MAX}, γ_{MAX} = values of the quantities Λ, ζ, γ under conditions of maximum loading attainable in an idealized rotating actuator. --

Subsection 9.15

β_d = relative angle of flow at radius r_d on downstream side of actuator as defined in Eqs. (9.15.1) or (9.15.4). rad

β = relative angle of flow at relative radius η in remote slipstream as defined by Eq. (9.15.5). rad

η_m = mean radius ratio as defined by Eq. (9.15.6). --

Section 11

η = overall efficiency of real actuator as defined by Eq. (11.1.). --

η_i = efficiency of ideal actuator as defined by Eq. (11.1.2). --

e_N = rotation power effectiveness as defined by Eq. (11.2.1). --

e_r = residual power effectiveness as defined by Eq. (11.2.2). --

e_P = overall power effectiveness as defined by Eqs. (11.2.3) or (11.5). --

e_F = force effectiveness as defined by Eq. (11.6.2). --

e_B = braking effectiveness as defined by Eq. (11.6.3). --

$\left.C_{lF}\right)_{MAX}$ = maximum value of C_{lF} for an ideal actuator at a specified value of C_{lP}. --

$\left.C_{lF}\right)_{MAX}$ = minimum value of C_{lF} for an ideal actuator at a specified value of C_{lP}. --

5. Momentum and Energy Analysis of Idealized Zero Torque Actuator in Modes P, W and R

For all three of the flow configurations P, W and R considered in this section, there are four major reference stations within each stream, designated respectively by subscripts 0, u, d and s. The velocities, pressures and total flow energies at these stations are designated as shown in Table 5.1.

Table 5.1 Velocity, Pressure and Energy at Principal Stations

Station	Location	Velocity	Static Pressure	Total Energy Per Unit Mass
0	Far upstream	V	p	E
u	At actuator, upstream side	$V_u = V_d$	p_u	E
d	At actuator, downstream side	V_d	p_d	$E + \Delta E$
s	Slipstream	$V_S = V + \Delta V$	p	$E + \Delta E$

It should be noted that the terms upstream and downstream in Table 5.1 and elsewhere in this discussion always refer to the effective flow through the actuator, not to the ambient flow field. Thus for reversed flow in mode R, the upstream station u is on the aft side of the actuator disc! Also note that by reason of continuity, the axial velocity must be equal at stations u and d and that the single symbol V_d is therefore used for both.

Bernoulli's equation can be applied firstly between stations 0 and u and secondly between stations s and d. Thus for any single mode we thereby obtain

$$E = \frac{p}{\rho} + \frac{V^2}{2} = \frac{p_u}{\rho} + \frac{V_d^2}{2} \qquad (5.1.1)$$

$$E + \Delta E = \frac{p}{\rho} + \frac{(V + \Delta V)^2}{2} = \frac{p_d}{\rho} + \frac{V_d^2}{2} \qquad (5.1.2)$$

Upon subtracting (5.1.1) from (5.1.2) and rearranging, we obtain the difference in total energy and in static pressure across the actuator disc in the form -

$$\rho \Delta E = \left(p_d - p_u\right) = \rho \left(V + \frac{\Delta V}{2}\right) \Delta V \qquad (5.2)$$

The present analysis is restricted to unshrouded configurations only. Thus the whole thrust F is produced by the above static pressure difference acting on the actuator disc area. However, the sense of the thrust depends on whether the sense of the flow through the disc is positive or negative.

We therefore express the result in the generalized form

$$F = \frac{\pi \varphi}{4} \rho D^2 \left(V + \frac{\Delta V}{2}\right) \Delta V \qquad (5.3)$$

where the operator φ assures that the force always has the correct algebraic sign.

A second independent expression for the thrust can also be found by applying the momentum theorem between stations 0 and s. For this purpose we need the absolute mass flow rate through the actuator which can be expressed in the form

$$\dot{m} = \frac{\pi}{4} \rho D^2 \left|V_d\right| = \frac{\pi \varphi}{4} \rho D^2 V_d \qquad (5.4)$$

Consequently the required thrust may be finally written as

$$F = \frac{\pi \varphi}{4} \rho D^2 V_d \Delta V \qquad (5.5)$$

Comparison of Eqs. (5.3) and (5.5) now reveals that algebraically

$$V_d = V + \frac{\Delta V}{2} \qquad (5.6)$$

For the idealized actuator, the shaft power P_i goes entirely into changing the total energy of the fluid which passes through it. Thus the algebraic shaft power P_i equals the product of the algebraic energy change ΔE as expressed in Eq. (5.2) with the absolute mass flow rate $\dot{m}$ as given by Eq. (5.4). Therefore, using Eq. (5.6) to eliminate V_d, we finally obtain for the power

$$P_i = \frac{\pi\varphi}{4} \rho D^2 \left(V + \frac{\Delta V}{2}\right)^2 \Delta V \tag{5.7}$$

At this point the key relations applicable to modes P, W and R can be summarized as follows:

$$V_S = V + \Delta V \tag{5.8.1}$$

$$V_d = V + \frac{\Delta V}{2} \tag{5.8.2}$$

$$\varphi = \frac{V_d}{|V_d|}$$

and

$$F = \frac{\pi\varphi}{4} \rho D^2 \left(V + \frac{\Delta V}{2}\right) \Delta V \tag{5.9.1}$$

$$P_i = \frac{\pi\varphi}{4} \rho D^2 \left(V + \frac{\Delta V}{2}\right)^2 \Delta V \tag{5.9.2}$$

Eqs. (5.9) define the fundamental relation among the principal quantities ρ, A, V, F and P_i in terms of the auxiliary parameter ΔV. While it is not mandatory to do so, it is in some respects convenient to eliminate this secondary parameter ΔV between the two relations (5.9). The result may be written

$$F^3 = \frac{\pi\varphi}{2} \rho D^2 P_i (P_i - FV) \tag{5.10.1}$$

We note that this equation is linear in V, quadratic in P_i and cubic in F. Hence explicit solutions for V or P_i may be readily obtained, but an explicit solution for F, while entirely feasible, turns out to be more involved. We shall not undertake the cubic solution for F at this point. However, solving Eq. (5.10.1) for V gives

$$V = \frac{P_i}{F} - \frac{2}{\pi\varphi}\left(\frac{F^2}{\rho D^2 P_i}\right) \tag{5.10.2}$$

Likewise, solving Eq. (5.10.1) for P_i we obtain two roots. Nevertheless, by use of the operator σ_i, the solution may be expressed unambiguously as follows.

$$P_i = \left(\frac{FV}{2}\right) + \sigma_i \sqrt{\left(\frac{FV}{2}\right)^2 + \frac{2}{\pi\varphi}\left(\frac{F^3}{\rho D^2}\right)} \tag{5.10.3}$$

It is shown in a later section that the formal analytical solution defined by Eqs. (5.9), or by Eqs. (5.10.1) or (5.10.2), consists of four distinct branches. Three of these correspond respectively to modes P, W and R. The fourth branch is extraneous; it represents a theoretical solution, mode U, which is actually unstable for any unshrouded configuration. One advantage of the particular form of solution defined by Eq. (5.10.3) is that by reason of the selective character of the operator σ_i, this extraneous branch is eliminated.

It is also instructive to analyze the basic momentum energy relations with respect to axes which, instead of being fixed with respect to the actuator itself as assumed heretofor, are fixed instead in the remote fluid. In this axis system, the actuator is moving with velocity V. The reaction force of amount F exerted by the fluid upon the actuator therefore delivers a thrust power of amount FV. Of course, this may be positive or negative thrust power, depending on the sign of F.

In addition, the velocities at stations 0 and s with respect to the new axes are now zero and ΔV, respectively. The corresponding total energies per unit mass are $\frac{p}{\rho}$ and $\left[\frac{p}{\rho} + \frac{(\Delta V)^2}{2}\right]$, respectively. Hence the net change in total energy per unit mass is the difference between these two quantities or $\frac{(\Delta V)^2}{2}$. This is simply the kinetic energy per unit mass of the slipstream with respect to the new axes. Since the slipstream flow is being "generated" at the rate of $\dot{m}$ units of mass per unit time, the creation of this kinetic energy in the slipstream consumes power at the rate $P_S = \dot{m}\frac{(\Delta V)^2}{2}$. Of course the power P_S imparted to the slipstream represents a loss of useful power which is basic and unavoidable, even for an actuator which is, by definition, completely idealized. Moreover, since the thrust power FV, the power P_S lost to the slipstream, and the shaft power P_i must satisfy an overall energy balance, we may write at once that

$$P_S = \left(P_i - FV\right) = \dot{m}\frac{(\Delta V)^2}{2} \geq 0 \qquad (5.11.1)$$

By utilizing Eqs. (5.4) and (5.5), this relation can readily be amplified to reveal that

$$P_S = \left(P_i - FV\right) = \frac{F\Delta V}{2} = \dot{m}\frac{(\Delta V)^2}{2} \geq 0 \qquad (5.11.2)$$

This relation in terms of the quantity $\frac{F\Delta V}{2}$ can also be obtained independently by dividing Eq. (5.9.2) by (5.9.1) and rearranging. This agreement provides further confirmation of Eqs. (5.11.1) and (5.11.2). It also shows that the power analyses in the two different axis systems are mutually consistent.

It is significant that the separate quantities P_i and FV can be either positive or negative, but that the difference $(P_i - FV)$ must always remain non-negative. As explained above, this quantity represents an irreducible minimum loss of power which is unavoidable even with an ideal actuator.

Naturally, for any real actuator operating with corresponding values of ρ, D, V and F, the actual power loss must be even greater than this basic minimum.

By rearranging Eqs. (5.10.1) and (5.10.3) we can also find two alternative and equivalent expressions for the basic power loss in terms that are frequently more convenient than the original form (5.11.2). They are, respectively,

$$P_S = \left(\frac{F\Delta V}{2}\right) = \left(\frac{2}{\pi\varphi}\right)\left(\frac{F^3}{\rho D^2 P_i}\right) \geq 0 \qquad (5.11.3)$$

and

$$P_S = \left(\frac{F\Delta V}{2}\right) = \left\{\sigma_i \sqrt{\left(\frac{FV}{2}\right)^2 + \frac{2}{\pi\varphi}\left(\frac{F^3}{\rho D^2}\right)} - \frac{FV}{2}\right\} \geq 0 \qquad (5.11.4)$$

Once again, the sign of the radical in Eq. (5.11.4) is specified by the operator σ_i in such a way as to eliminate the physically extraneous branch of the solution.

Notice that the above results, Eqs. (5.8.1) through (5.11.4) have been established in a form which does not involve division by V in any term. Hence the solution for the important special case of static thrust may be found simply by substituting V = 0 into these equations. In this case we also find that since thrust power vanishes,

$$P_i = P_S \qquad (5.12)$$

It may be remarked in passing that a fan, unlike a propeller, windmill or lifting rotor, is utilized for the very purpose of creating a moving slipstream. Hence the power P_S imparted to the slipstream, which must be regarded as a dead loss for these other three devices, becomes the principal useful output for the fan! Apart from this single change in purpose and viewpoint, the analysis of the idealized fan is exactly the same as that given here for these other actuators.

The fundamental result of this section is the basic actuator relation, Eq. (5.10.3). Alternatively, we may choose either of the equivalent forms (5.10.1) or (5.10.2). The same basic relation is also defined by the pair of parametric equations, (5.9.1) and (5.9.2), in which ΔV plays the role of auxiliary parameter.

On the other hand for the exceptional case of a fan, the basic relation between output P_S and input P_i is summarized parametrically by the pair of equations, (5.11.3) and (5.10.3), in which F now plays the role of auxiliary parameter.

The foregoing fundamental results, in any or all of the above forms, may be further simplified by non-dimensionalization. This process reduces the number of parameters finally involved by three. The results previously summarized in section 2.0 were developed in this way.

Eq. (5.10.1) which is cubic in F, is not solved explicitly for F in this section. However, the cubic solution has been worked out in detail and presented in connection with several of the non-dimensional forms summarized in section 2.0.

6. Stable and Unstable Branches of the Formal Solution

It is useful at this point to non-dimensionalize the foregoing results in terms of the dimensional reference parameters ρ, D, V. For this purpose we define the following dimensionless coefficients, namely,

$$C_{lF} = \frac{F}{\rho D^2 V^2} \tag{6.1.1}$$

$$C_{lPi} = \frac{P_i}{\rho D^2 V^3} \tag{6.1.2}$$

$$\lambda = \frac{\Delta V}{V} \tag{6.1.3}$$

In terms of these coefficients, the detailed formal solution represented by Eqs. (5.8.1) through (5.11.4) may be summarized in dimensionless form as follows.

$$\left(\frac{V_s}{V}\right) = 1 + \lambda \tag{6.2.1}$$

$$\left(\frac{V_d}{V}\right) = 1 + \frac{\lambda}{2} \tag{6.2.2}$$

$$\varphi = \frac{\left(1 + \frac{\lambda}{2}\right)}{\left|1 + \frac{\lambda}{2}\right|} \tag{6.2.3}$$

$$C_{lF} = \frac{\pi\varphi}{4}\left(1 + \frac{\lambda}{2}\right)\lambda \tag{6.3.1}$$

$$C_{lPr} = \frac{\pi\varphi}{4}\left(1 + \frac{\lambda}{2}\right)^2 \lambda \tag{6.3.2}$$

$$C_{lF}{}^3 = \frac{\pi\varphi}{2} C_{lPi}\left(C_{lPi} - C_{lF}\right) \tag{6.4.1}$$

$$C_{lPi} = \left(\frac{C_{lF}}{2}\right) + \sigma_i \sqrt{\left(\frac{C_{lF}}{2}\right)^2 + \frac{2}{\pi\varphi} C_{lF}{}^3} \tag{6.4.2}$$

The last three of these equations as given below represent alternative expressions for the dimensionless power loss to the slipstream.

$$\frac{C_{lF}\,\lambda}{2} = \left(C_{lPi} - C_{lF}\right) \tag{6.5.1}$$

$$\frac{C_{lF}\,\lambda}{2} = \frac{2}{\pi\varphi}\frac{C_{lF}{}^3}{C_{lPi}} \tag{6.5.2}$$

$$\frac{C_{1F}\,\lambda}{2} = \left\{ \sigma_i \sqrt{\left(\frac{C_{1F}}{2}\right)^2 + \frac{2}{\pi\varphi} C_{1F}^{\,3}} - \frac{C_{1F}}{2} \right\} \qquad (6.5.3)$$

The velocity ratios $\left(\frac{V_s}{V}\right)$ and $\left(\frac{V_d}{V}\right)$ as expressed by Eqs. (6.2) are plotted as functions of parameter λ in Fig. 6.1. The corresponding relation between C_{1F} and C_{1Pi}, as defined parametrically by Eqs. (6.3) or explicitly by Eq. (6.4.1), is plotted in Fig. 6.2.

Study of these charts discloses the existence of four distinct branches of the formal solution which are correlated with the previously defined modes as follows:

Branch $\overline{SO}$ - Mode P (Propulsion)

Branch $\overline{OMN}$ - Mode W (Windmill)

Branch $\overline{NUV}$ - Mode U (Unstable)

Branch $\overline{VCS'}$ - Mode R (Reversed Flow)

To see that branch $\overline{NUV}$ represents a physically unstable mode, we take note of the following facts. For this branch, parameter λ lies between -1 and -2. Eqs. (6.2) and Fig. 6.1 then show that the flow through the actuator is in the same sense as the ambient flow while the final flow in the remote slipstream is reversed with respect to the ambient flow. Thus the flow reversal takes place <u>after</u> the fluid passes through the actuator. Moreover, Eqs. (6.3) and Fig. 6.2 show that C_{1F} and C_{1Pi} are both negative in this range. In other words the actuator sustains a drag force and extracts useful power from the stream which subsequently reverses and departs in a sense opposite to that of the ambient flow.

While the above behavior would theoretically be possible within the confines of a properly designed channel with physical restraining walls, it cannot be sustained in the unrestrained environment of an unshrouded actuator. The

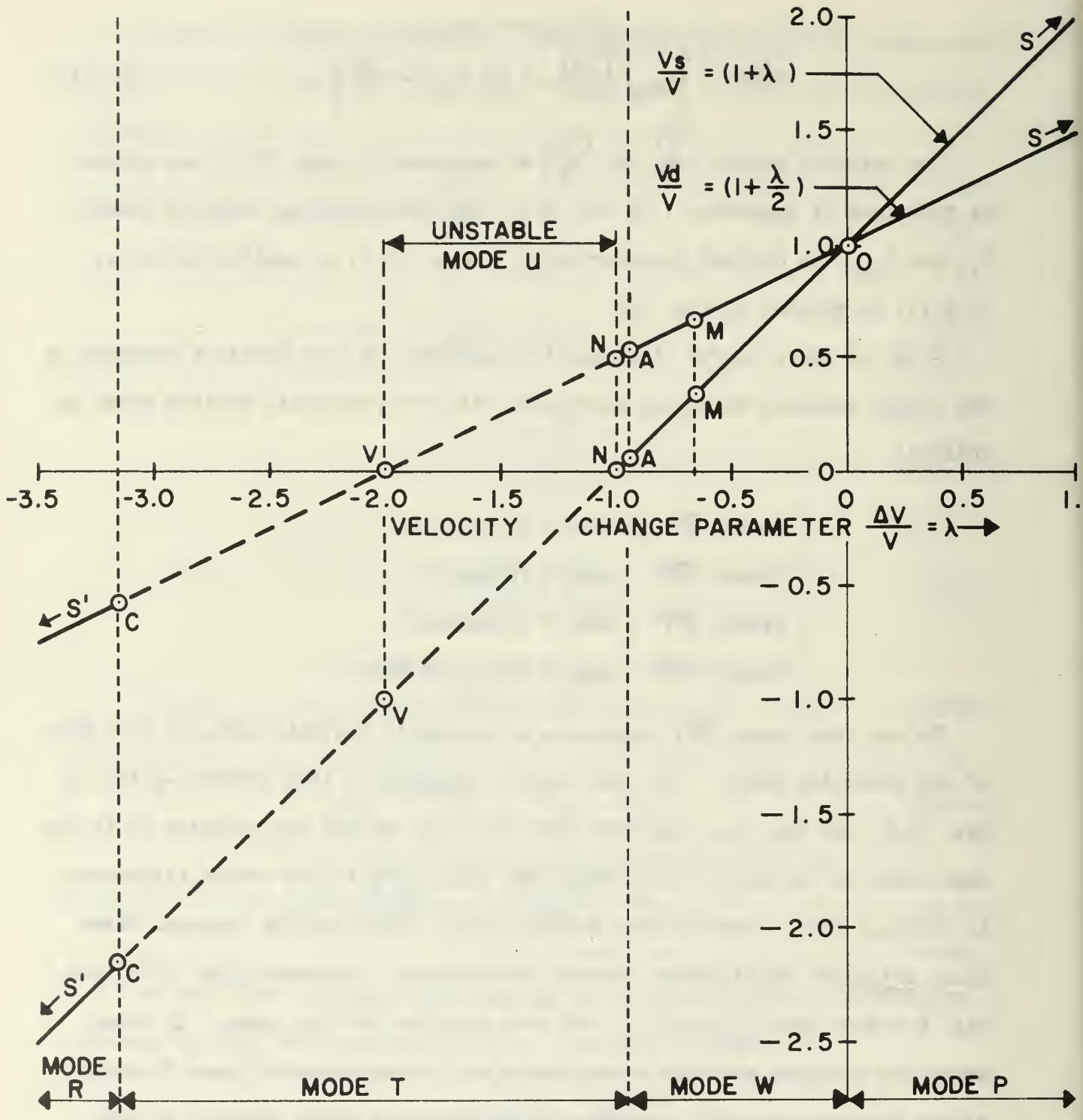

Fig. 6.1 VELOCITY RATIOS IN SLIPSTREAM AND AT ACTUATOR DISC AS FUNCTIONS OF VELOCITY CHANGE PARAMETER λ.

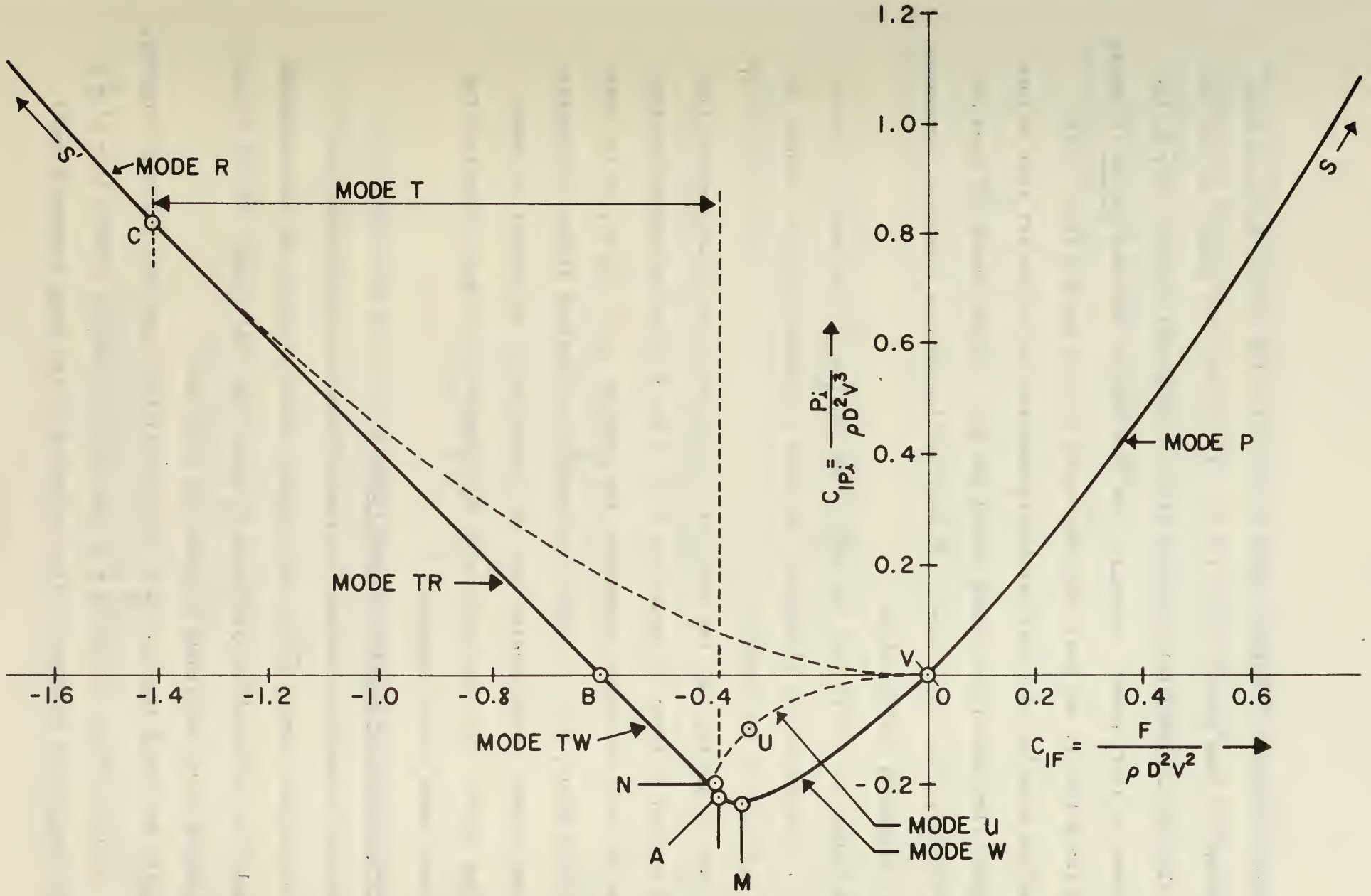

Fig. 6.2 IDEAL PERFORMANCE ENVELOPE IN ρ, D, V SYSTEM.

mechanism of vorticity transport which causes this flow pattern to break down is discussed in some detail in section 8. It suffices here merely to point out that a flow can be completely reversed with an unshrouded actuator only by the expenditure of shaft power. Actually, the flow must be reversed before it passes through the actuator, and must therefore enter it from the aft side. This requires the creation of a sufficiently intense suction on the aft side to turn the ambient flow inward and around toward the disc. Since branch $\overline{NUV}$ does not satisfy these various requirements, it must be discarded as physically irrelevent for any unshrouded configuration.

The reader can verify that the analytical solution in the specific form of Eq. (6.4.2) automatically eliminates the above extraneous solution through the selective action of the operator σ_i.

We note in passing that the detailed solution which is non-dimensionalized in this section in terms of parameters ρ, D, V can also be non-dimensionalized in terms of other reference parameters, for example, ρ, D, $|P|$ or, in the case of a lifting rotor, ρ, D, L. While the results so obtained differ in algebraic form, they express relationships that are theoretically equivalent to those summarized above. The form based on ρ, D, V happens to be most convenient for the present phase of the analysis.

7. A New Solution for Transition Range, Mode T

Since the transition from mode W to mode R cannot actually take place along the unstable branch $\overline{NUV}$ of the original formal solution, we are compelled to formulate an alternative hypothesis to apply over this range. We now propose the following novel yet simple solution for this case.

Imagine the total disc area $\frac{\pi}{4} D^2$ to be subdivided into two concentric regions, namely, an inner circle of area $x \frac{\pi}{4} D^2$ and an outer annulus of area $(1 - x) \frac{\pi}{4} D^2$ where the transition parameter x lies somewhere in the range between 0 and 1.

We assume that the flow over the inner region corresponds to some as yet unspecified operating point A of mode W, and that flow over the outer region corresponds to some as yet unspecified operating mode point C of mode R.

Consider the following relations.

For the inner flow -

$$-1 \leq \lambda_A \leq 0 \tag{7.1.1}$$

$$C_{lFA} = + \frac{\pi}{4} \left(1 + \frac{\lambda_A}{2}\right) \lambda_A \tag{7.1.2}$$

$$C_{lPiA} = + \frac{\pi}{4} \left(1 + \frac{\lambda_A}{2}\right)^2 \lambda_A \tag{7.1.3}$$

For the outer flow -

$$- \infty \leq \lambda_C \leq - 2 \tag{7.2.1}$$

$$C_{lFC} = - \frac{\pi}{4} \left(1 + \frac{\lambda_C}{2}\right) \lambda_C \tag{7.2.2}$$

$$C_{lPiC} = - \frac{\pi}{4} \left(1 + \frac{\lambda_C}{2}\right)^2 \lambda_C \tag{7.2.3}$$

The corresponding net overall values for the combined flow are found simply by adding the respective contributions from the inner and outer streams. The results are

$$C_{lF} = x\, C_{lFA} + (1 - x)\, C_{lFC} \tag{7.3.1}$$

$$C_{lPi} = x\, C_{lPiA} + (1 - x)\, C_{lPiC} \tag{7.3.2}$$

Upon eliminating x between these last two relations we obtain

$$C_{lPi} = C_{lPiC} + \left[\frac{C_{lPiA} - C_{lPiC}}{C_{lFA} - C_{lFC}}\right]\left(C_{lF} - C_{lFC}\right) \tag{7.4}$$

The result shows that for fixed values of λ_A and λ_C, the relation between C_{lPi} and C_{lF} is linear over the transition range.

The problem that remains is to find the values of the parameters λ_A and λ_C such as to optimize actuator performance over the transition range. This means that for any given value of C_{lF}, the power coefficient C_{lP}, whether positive or negative, should be algebraically as small as possible. Inspection of Fig. 6.2 shows that this requirement is satisfied simply by choosing as the transition line the straight line segment $\overline{AC}$ which is tangent to the original analytical curve at the two points A and C as shown.

In this connection we note that the slope of the original curve at these two points can be expressed in the form

$$\left(\frac{d\,C_{lPi}}{d\,C_{lF}}\right)_A = S_A = \frac{\left(1 + \frac{\lambda_A}{2}\right)\left(1 + \frac{3\lambda_A}{2}\right)}{(1 + \lambda_A)} \tag{7.5.1}$$

$$\left(\frac{d\,C_{lPi}}{d\,C_{lF}}\right)_C = S_C = \frac{\left(1 + \frac{\lambda_C}{2}\right)\left(1 + \frac{3\lambda_C}{2}\right)}{(1 + \lambda_C)} \tag{7.5.2}$$

Furthermore, the slope of the straight line segment joining points A and C can be reduced to the form

$$S = \left[\frac{\left(1 + \frac{\lambda_A}{2}\right)^2 \lambda_A + \left(1 + \frac{\lambda_C}{2}\right)^2 \lambda_C}{\left(1 + \frac{\lambda_A}{2}\right)\lambda_A + \left(1 + \frac{\lambda_C}{2}\right)\lambda_C}\right] \tag{7.5.3}$$

Now the optimizing condition requires simply that

$$S = S_A = S_C \tag{7.5.4}$$

Simultaneous solution of Eqs. (7.5) gives the following important results -

$$S = S_A = S_C = -1 \tag{7.6.1}$$

$$\lambda_A = -2\left(\frac{\sqrt{3} - 1}{\sqrt{3}}\right) = -0.845 \tag{7.6.2}$$

$$\lambda_C = -2\left(\frac{\sqrt{3} + 1}{\sqrt{3}}\right) = -3.155 \tag{7.6.3}$$

Therefore Eqs. (7.1) and (7.2) give at point A -

$$C_{lFA} = -\frac{\pi}{6}(\sqrt{3} - 1) = -0.382 \tag{7.7.1}$$

$$C_{lPiA} = -\frac{\pi}{6}\left(\frac{\sqrt{3} - 1}{\sqrt{3}}\right) = -0.222 \tag{7.7.2}$$

At point C -

$$C_{lFC} = -\frac{\pi}{6}(\sqrt{3} + 1) = -1.43 \tag{7.7.3}$$

$$C_{lPiC} = +\frac{\pi}{6}\left(\frac{\sqrt{3} + 1}{\sqrt{3}}\right) = +0.825 \tag{7.7.4}$$

Consequently, the resulting solution over the transition range as represented by Eq. (7.4) can now be reduced to the final form

$$C_{lPi} = -\frac{\pi}{3\sqrt{3}} - C_{lF} \tag{7.8.1}$$

which applies over the range

$$-\frac{\pi}{6}(\sqrt{3}+1) \leq C_{1F} \leq -\frac{\pi}{6}(\sqrt{3}-1) \qquad (7.8.2)$$

8. Propagation of Vorticity and Development of the Vortex Ring State

Consider conditions at station s far downstream of the actuator. The slipstream at this location is moving with uniform velocity V_S, the ambient flow with uniform axial velocity V. In the idealized inviscid case, the two irrotational flow regions are separated by a vortex sheet of infinitesimal thickness in the form of a cylindrical surface. The vortex lines are circumferential; the surface consists of a continuous distribution of vortex rings. According to the Helmholtz laws of vortex motion for an inviscid fluid, the circulation moves with the fluid element which exhibits it. These rotating fluid elements which constitute the interfacial vortex sheet themselves move with a velocity V_ω which is the algebraic mean of the velocities V and V_S on either side of the interface, thus

$$V_\omega = \tfrac{1}{2}(V + V_S) \qquad (8.1.1)$$

By comparing this with Eq. (5.8.2) we note that

$$V_\omega = V_d \qquad (8.1.2)$$

In other words the velocity of propagation V_ω of the remote vorticity is the same as the flow velocity V_d through the disc itself! This applies also to the transition mode T if we consider the inner and outer streams individually.

We may view the vortex rings as vorticity shed originally from the actuator disc and propagated at an eventual axial velocity $V_\omega = V_d$. Normally, the propagation is in the sense leading away from the actuator, which tends to produce a stable flow pattern. If the sense of propagation should become reversed for

any reason so that the vortex rings were to move toward the actuator disc, the tendency would be to disrupt the original flow pattern. All of the vorticity would tend to collect and become fixed at the actuator, thus leading to the establishment of the vortex ring regime as shown earlier in the schematic diagram Fig. 2.6.3.

This idea can easily be reduced to explicit mathematical terms. Consider firstly flows like modes P and W in which the slipstream continues in the same sense as the undisturbed flow. In this case

$$\frac{V_s}{V} = (1 + \lambda) > 0 \qquad (8.2.1)$$

and stability in the above sense requires that

$$\frac{V_d}{V} = \left(1 + \frac{\lambda}{2}\right) > 0 \qquad (8.2.2)$$

Next consider flows like mode R in which the slipstream is reversed with respect to the undisturbed flow. In this case

$$\frac{V_s}{V} = (1 + \lambda) < 0 \qquad (8.2.3)$$

and stability requires that

$$\frac{V_d}{V} = \left(1 + \frac{\lambda}{2}\right) < 0 \qquad (8.2.4)$$

The above conditions may be consolidated into the single statement that, for stability, it is necessary that

$$\frac{1 + \frac{\lambda}{2}}{1 + \lambda} > 0 \tag{8.3.1}$$

It can be seen that the stability constraint (8.3.1) is satisfied for all values of λ except those lying within the range

$$-2 \leq \lambda \leq -1 \tag{8.3.2}$$

But this is precisely the range of the mode U which was previously identified as the unstable branch of the formal solution!

Of course, the two end points identified in Eq. (8.3.2) are points of neutral stability. We identify these as points V and N, respectively. Note that

<u>At Point N</u>

$$\lambda = -1 \tag{8.4.1}$$

$$C_{lF} = \frac{\pi\varphi}{4}\left(1 + \frac{\lambda}{2}\right)\lambda = -\frac{\pi}{8} \tag{8.4.2}$$

$$C_{lPi} = \frac{\pi\varphi}{4}\left(1 + \frac{\lambda}{2}\right)^2\lambda = -\frac{\pi}{16} \tag{8.4.3}$$

<u>At Point V</u>

$$\lambda = -2 \tag{8.5.1}$$

$$C_{lF} = 0 \tag{8.5.2}$$

$$C_{lPi} = 0 \tag{8.5.3}$$

It is of interest to compare this latter point with another significant operating condition, namely, point O. Thus

At Point O $\lambda = 0$ (8.6.1)

$$C_{lF} = 0 \tag{8.6.2}$$

$$C_{lPi} = 0 \tag{8.6.3}$$

This brings out the very interesting fact that although points O and V are both located at the origin in the C_{lPi} versus C_{lF} plane, they represent quite distinct operating conditions. In particular, point O is a state of positive stability while point V is a state of neutral stability. In fact, point V represents the vortex ring state previously mentioned. A rotorcraft which is inadvertantly brought to this operating point suddenly suffers a catastropic loss of lift!

Consider in this light the operation of an actuator, initially in mode R, at gradually decreasing levels of power coefficient C_{lPi}. Assume that when the actuator reaches point C, operation is not shifted along the optimum transition path CBA, but is controlled so as to continue along in mode R toward point V. It can be seen that as the operating point moves closer to point V, the margin of stability in the above sense becomes less until at point V itself, the point of incipient instability is finally reached. It is evident that for operation unduly close to this point, a quite small perturbation may suffice to disrupt the precarious stability, and lead to the vortex ring state.

Moreover, if the attempt were nevertheless made to continue the above gradual changes further into the unstable region $\overline{VUN}$, the resulting unstable flow pattern would inevitably collapse, to be succeeded in most cases by the vortex ring pattern.

In contrast with this, during a shift along the optimum transition path CBA, operation too near the points of incipient instability, V and N, is avoided. Hence path CBA is theoretically stable in this sense as well as being the transition path of highest performance.

Of course, for a real actuator, there may be various other types of instabilities to consider. Fortunately, these are usually of a less drastic kind. Even for the idealized actuator, however, there are other types of instabilities as well. One particular type is analyzed in section 10 of this paper. In general, however, the phenomena of hydrodynamic instability in real systems are extremely complex and cannot be analyzed by the elementary methods of this paper.

9. Rotation Effects on Actuator Performance

9.1 The Idealized Finite Torque Actuator

The ideal actuator considered so far involves purely axial flow in the remote slipstream and is, in effect, a zero torque device. In principle, this condition could be approximated in various ways. One method would be to use a pair of co-axial counter-rotating rotors which exert equal and opposite torques upon the flow. Another method would be to use a rotor and a co-axial stator which exert equal and opposite torques. A third method would be to utilize a single rotor at rotational speeds so high that the necessary power could be transmitted at torque levels low enough to be negligible.

In most cases, the above methods are for one reason or another impractical, and it becomes useful to consider in somewhat greater detail the optimum performance which can be attained by a single rotation actuator which transmits appreciable shaft power at limited rotational speed and therefore with significant torque effects. In general such a device, which we term here the

finite torque actuator, even if idealized in every other respect, will always perform somewhatless effectively than the comparable idealized zero torque actuator.

9.2 Idealized Rotation Power Loss

Consider three actuators all of which operate with the same values of ρ, D, V and F, respectively, but with different values of shaft power P. The first is the ideal zero torque actuator with ideal shaft power P_i as previously analyzed. The second is an idealized finite torque actuator and the third is the real actuator; both of these latter devices operate at the same shaft speed N. The shaft power P_i' of the idealized finite torque actuator equals $(P_i + P_N)$ where P_N, which is always non-negative, is here termed the idealized rotation loss. The shaft power P of the real actuator was previously written as equal to $(P_i + P_f)$ where P_f, which is always non-negative, denotes the total power loss. This same total shaft power P can now be represented in somewhat more detail by the expression $(P_i + P_N + P_r)$ where P_r, which we term here the residual loss, is again a non-negative quantity. This analysis resolves the total power loss P_f into an idealized rotation loss P_N plus a residual loss P_r.

9.3 Conventional Coefficients in Terms of Slipstream Parameters

In the preceding discussion of power losses, it is necessary to distinguish between various power components and in this context the total shaft power of the idealized finite torque actuator is denoted by the somewhat elaborate symbol P_i'. However, in this and subsequent subsections, the discussion is restricted solely to the analysis of the idealized finite torque actuator itself, hence we elect to denote this same power P_i' hereafter by the simpler and more convenient symbol P. Consequently, the significant parameters of our problem are ρ, D, V, F, N and P. Note that this list now includes N, which is

non-vanishing, finite and positive. Hence it becomes advantageous to revert to the use of the conventional performance coefficients C_F, C_P and J based on ρ, N and D as dimensional reference parameters.

It is shown in a later subsection that the performance of the idealized finite torque actuator can be analyzed in terms of conditions in the remote slipstream, station s. It is necessary, of course, to distinguish between the diameter of the slipstream, which we here denote as 2R, and the diameter D of the actuator disc itself. It is also convenient to express shaft speed both in conventional units of rev/sec as denoted by N and in scientific units of rad/sec as denoted by ω. With this notation, the required performance coefficients may be expressed as follows:

$$C_F = \frac{F}{\rho N^2 D^4} = \frac{\pi^2}{4}\left(\frac{2R}{D}\right)^4 \left(\frac{F}{\rho \omega^2 R^4}\right) \tag{9.3.1}$$

$$C_P = \frac{P}{\rho N^3 D^5} = \frac{\pi^3}{4}\left(\frac{2R}{D}\right)^5 \left(\frac{P}{\rho \omega^3 R^5}\right) \tag{9.3.2}$$

$$J = \left(\frac{V}{ND}\right) = \pi\left(\frac{2R}{D}\right)\left(\frac{V}{\omega R}\right) \tag{9.3.3}$$

9.4 Basic Slipstream Analysis

An actuator which transmits shaft power P to an initially nonrotating stream, and which itself rotates at shaft angular velocity ω, necessarily exerts a torque of amount P/ω upon the flow. Assuming polar symmetry for the idealized flow model, we conclude that the above torque sets up in the remote slipstream a distribution of tangential velocity V_u which varies in some manner as a function of radius r. In general, the axial velocity V_s

in the remote slipstream can also vary as some function of r. The stream-surfaces of this flow are straight co-axial cylinders.

The pressure at the outer edge of the slipstream, radius R, equals the ambient pressure p. For a rotating slipstream, the pressure p_S at any interior radius r is below ambient. Considerations of radial balance of forces show that the amount of pressure drop is

$$\left(\frac{p - p_S}{\rho}\right) = \int_r^R \frac{V_u^2}{r}\, dr \qquad (9.4.1)$$

Applying the energy equation between a point in the slipstream and a point far upstream of the actuator, we find the net energy input to the flow to be

$$\Delta E = \left[\frac{p_S}{\rho} + \frac{V_S^2 + V_u^2}{2}\right] - \left[\frac{p}{\rho} + \frac{V^2}{2}\right] \qquad (9.4.2)$$

The energy input can also be written in terms of shaft power input per unit mass flow, where shaft power is expressed in terms of torque and angular velocity, and where torque is written in terms of change in angular momentum. The result is simply

$$\Delta E = \omega V_u r \qquad (9.4.3)$$

Upon combining these last three equations, we obtain the basic relation

$$\left(\frac{V_S^2 - V^2}{2}\right) = \omega V_u r - \frac{V_u^2}{2} + \int_r^R \frac{V_u^2}{r}\, dr \qquad (9.4.4)$$

This shows how the distributions of V_u and V_S in the slipstream must be related for any assigned values of the parameters V and ω.

9.5 Idealized Velocity Distribution in the Slipstream

Our basic aim is to find a distribution of V_u which will leave V_S unchanged from the result obtained for the original zero torque actuator. In other words, we require a V_u distribution which produces a uniform axial velocity V_S across the slipstream. Moreover, it must be possible to prescribe the magnitude of V_S arbitrarily.

It turns out that the required solution consists of two distinct regions. There is firstly a non-swirling inner core of radius r_0. Outside the core, there is an annular region of simple free vortex flow. Thus

For $0 \leq r \leq r_0$ $\quad V_u r = 0$ (9.5.1)

For $r_0 \leq r \leq R$ $\quad V_u r = \Gamma = \text{constant}$ (9.5.2)

Substituting V_u from Eq. (9.5.2) into (9.4.4) gives the result

$$\left(\frac{V_S^2 - V^2}{2}\right) = \omega \Gamma - \frac{\Gamma^2}{2R^2} \tag{9.5.3}$$

With all other quantities arbitrarily prescribed, this equation fixes the characteristic swirl constant Γ of the outer free vortex flow.

The total pressure drop through the outer annulus can now be found by substituting the free vortex relation (9.5.2) into the radial balance equation (9.4.1). The result is

$$\left(\frac{p - p_{SO}}{\rho}\right) = \frac{\Gamma^2}{2R^2}\left[\frac{R^2}{r_0^2} - 1\right] \tag{9.5.4}$$

For the flow through the nonrotating inner core, there is no net energy input and the energy equation gives

$$\left(\frac{V_S^2 - V^2}{2}\right) = \left(\frac{p - p_{SO}}{\rho}\right) \tag{9.5.5}$$

By eliminating the pressure term between these last two expressions, we obtain a solution for the core radius in the form

$$\frac{R^2}{r_0^2} = 1 + \frac{\left(\frac{V_S^2 - V^2}{2}\right)}{\left(\frac{\Gamma^2}{2R^2}\right)} \tag{9.5.6}$$

where Γ is now known from the prior solution of Eq. (9.5.3).

Eqs. (9.5.1) through (9.5.6) completely define all features of the slipstream flow which correspond to arbitrarily specified values of the parameters V_S, V and ω.

9.6 Slipstream Thrust Integral

Applying the axial momentum law to the propeller, we can now write the net thrust in the form of an integral over the slipstream as follows:

$$F = 2\pi\rho \int_0^R \left\{ V_S \left(V_S - V\right) - \int_r^R \frac{V_u^2}{r}\, dr \right\} r\, dr \tag{9.6.1}$$

The first term inside the integrand represents the basic thrust produced by the momentum increase across the actuator. The second term, which can be recognized as the pressure drop integral of Eq. (9.4.1), represents a loss of thrust associated with the lowered pressures near the axis. This equation also indicates why it is necessary to maintain a nonrotating core of adequate radius r_0. For if r_0 be allowed to decrease unduly, the unfavorable negative pressure integral eventually dominates the solution. The non-swirling core of radius r_0 eliminates this difficulty.

In fact, over the core of the present solution, the integrand of the thrust equation (9.6.1) reduces as follows

$$\left\{V_S\left(V_S - V\right) - \int_{r_0}^{R} \frac{V_u^2}{r}\,dr\right\} = \left\{V_S\left(V_S - V\right) - \left(\frac{V_S^2 - V^2}{2}\right)\right\}$$

$$= \tfrac{1}{2}\left(V_S - V\right)^2 > 0 \qquad (9.6.2)$$

It is interesting to observe from this result that the non-swirling core still makes a net positive contribution to the thrust despite the fact that it receives no energy input and undergoes no pressure rise in passing through the actuator! The reason, of course, is that it discharges as an axial jet into the region of reduced pressure created by the outer swirling flow. It exerts this thrust not as a pressure increase across the actuator, but as a suction force distributed along the converging stream surface which separates the inner and outer flows. The outer flow then transmits this force to the actuator disc itself.

9.7 Slipstream Power Integral

By integrating the energy relation (9.4.3) with respect to mass flow rate across the entire slipstream, the following expression is obtained for shaft power, namely,

$$P = 2\pi\,\rho\,\omega \int_{r}^{R} V_S\,V_u\,r^2\,dr \qquad (9.7.1)$$

Likewise, from (9.4.1) and (9.4.2) we can obtain the alternative form

$$P = 2\pi\rho \int_{0}^{R} \left\{\left(\frac{V_S^2 - V^2}{2}\right) + \left[\frac{V_u^2}{2} - \int_{r}^{R} \frac{V_u^2}{r}\,dr\right]\right\} r\,dr \qquad (9.7.2)$$

The form (9.7.1) is much simpler to compute , but (9.7.2) is interesting theoretically, especially in conjunction with the force equation (9.6.1). Notice that the effect of the terms in V_u is to decrease the thrust delivered and simultaneously to increase the shaft power required! The adverse effect of slipstream rotation on overall performance is at once evident from these formulas. Fortunately, at sufficiently high shaft speeds, these effects become small.

9.8 Non-dimensional Slipstream Parameters

In applying the foregoing results it is useful to non-dimensionalize all slipstream quantities and relations initially in terms of the three dimensional reference parameters ρ, ω and R. In this connection we introduce the following dimensionless quantities, namely,

$$\frac{V}{\omega R} = \varkappa \qquad \text{Slipstream advance ratio} \qquad (9.8.1)$$

$$\frac{\left(V_S - V\right)}{\omega R} = \Lambda \qquad \text{Slipstream loading parameter} \qquad (9.8.2)$$

$$\frac{\Gamma}{\omega R^2} = \gamma \qquad \text{Slipstream swirl parameter} \qquad (9.8.3)$$

$$\frac{r}{R} = \eta \qquad \text{Slipstream relative radius} \qquad (9.8.4)$$

Integration of Eqs. (9.6.1) and (9.7.1) in this system then yields solutions for the following two coefficients, namely,

$$\frac{F}{\rho\, \omega^2\, R^4} = \text{Slipstream force coefficient} \qquad (9.8.5)$$

$$\frac{P}{\rho\, \omega^3\, R^5} = \text{Slipstream power coefficient} \qquad (9.8.6)$$

9.9 Slipstream Contraction or Expansion

A glance at Eqs. (9.3) now shows that to convert the slipstream force and power coefficients into the conventional force and power coefficients C_F and C_P, and to convert slipstream advance ratio $\varkappa$ to the conventional advance ratio J, it is necessary to know the slipstream area contraction ratio $\left(\frac{2R}{D}\right)^2$.

Applying the continuity condition between actuator disc and slipstream gives the general result

$$\left(\frac{2R}{D}\right)^2 = \frac{\int_0^{D/2} V_d \, r_d \, dr_d}{\int_0^R V_S \, r \, dr} \tag{9.9.1}$$

However, for the specific solution developed in this section, the addition of the peripheral velocity components V_u in the slipstream does not affect the original axial velocity V_S. In fact the solution was specifically tailored to meet this requirement. For incompressible flows having polar symmetry, a free vortex motion superimposed on an arbitrary axial motion does not affect the latter. This principle is well known in fluid mechanics and is simply utilized here without detailed derivation or proof. We merely note that the superimposed free vortex motion does not affect the axial velocity distribution V_d. Also, since V_S and V_d both happen to be constants, Eq. (9.9.1)simplifies to

$$\left(\frac{2R}{D}\right)^2 = \frac{V_d}{V_S} = \frac{V + \frac{\Delta V}{2}}{V + \Delta V} \tag{9.9.2}$$

Upon non-dimensionalizing this in the ρ, ω, r system we obtain finally

$$\left(\frac{2R}{D}\right)^2 = \frac{\varkappa + \frac{\Lambda}{2}}{\varkappa + \Lambda} \tag{9.9.3}$$

9.10 Swirl Intensity, Loading Limit and Net Operating Range

Further details of the non-dimensionalized solution now work out as follows. The basic relation (9.5.3) which fixes slipstream swirl intensity takes the form

$$\left(\varkappa + \frac{\Lambda}{2}\right) \Lambda = \gamma - \tfrac{1}{2} \gamma^2 \tag{9.10.1}$$

It is useful to solve this for γ by the quadratic formula, and to arrange the resulting solution in the following special form, namely,

$$\gamma = \zeta \left(\varkappa + \frac{\Lambda}{2}\right) \Lambda \tag{9.10.2}$$

where the auxiliary parameter ζ is defined by the expression

$$\zeta = \left\{ \frac{1 - \sqrt{1 - 2 \left(\varkappa + \frac{\Lambda}{2}\right) \Lambda}}{\left(\varkappa + \frac{\Lambda}{2}\right) \Lambda} \right\} \tag{9.10.3}$$

It is also convenient for some purposes to expand this solution into series form as follows.

$$\zeta = 1 + \tfrac{1}{2} \left(\varkappa + \frac{\Lambda}{2}\right) \Lambda + \tfrac{1}{2} \left(\varkappa + \frac{\Lambda}{2}\right)^2 \Lambda^2 + \text{-----} \tag{9.10.4}$$

Inspection of Eq. (9.10.3) discloses an important physical operating limit. Since ζ is always real, the quantity under the radical can never become negative. We conclude that

$$\left[\left(\varkappa + \frac{\Lambda}{2}\right)\right] \Lambda_{\,MAX} = \tfrac{1}{2} \tag{9.10.5}$$

whereupon

$$\zeta\Big)_{MAX} = 2 \tag{9.10.6}$$

and

$$\gamma\Big)_{MAX} = 1 \tag{9.10.7}$$

Solving Eq. (9.10.5) for the loading limit Λ_{MAX} by the quadratic formula gives the result

$$\Lambda_{MAX} = + \sqrt{1 + \varkappa^2} - \varkappa \tag{9.10.8}$$

There is also a negative root for Λ which would be significant if we were considering reversed flows, mode R, in this analysis. However, the present discussion is limited to the simple modes P and W only, and in this context the negative root is not relevant.

On the other hand there is another restriction on Λ arising from the very fact that the analysis of this section is specifically limited to modes P and W. In terms of the earlier parameter λ, we may say that the present study is restricted to the range

$$-2 \left(\frac{\sqrt{3} - 1}{\sqrt{3}} \right) \leq \lambda \leq + \infty \tag{9.10.9}$$

where

$$\lambda = \frac{\Delta V}{V} = \frac{\Lambda}{\varkappa} \tag{9.10.10}$$

Upon combining these conditions, we find that the present analysis is restricted to the net operating range

$$- 2 \left(\frac{\sqrt{3} - 1}{\sqrt{3}} \right) \varkappa \leq \Lambda \leq + \sqrt{1 + \varkappa^2} - \varkappa \tag{9.10.11}$$

where positive values of Λ correspond to mode P, negative values to mode W.

9.11 Slipstream Core Radius

For any arbitrarily assigned values of $\varkappa$ and Λ which satisfy the constraint (9.10.11), parameter ζ is fixed by (9.10.3) or (9.10.4) and parameter γ by (9.10.2). Eq. (9.5.6) which fixes the relative radius η_0 of the non-swirling core in the slipstream can then be non-dimensionalized in the form

$$\frac{1}{\eta_0^2} = 1 + \frac{2}{\zeta\gamma} \tag{9.11.1}$$

9.12 Parametric Solution for Conventional Performance Coefficients

With all of the foregoing details fixed, it is a routine matter to non-dimensionalize and integrate the fundamental thrust and power relations (9.6.1) and (9.7.1). Upon utilizing relations (9.3), we finally obtain the following parametric solutions for C_F, C_P and J.

$$C_F = \frac{\pi^3}{4}\left(\frac{\kappa + \frac{\Lambda}{2}}{\kappa + \Lambda}\right)^2 \left\{(\kappa + \Lambda)\,\Lambda\left(1 - \eta_0^2\right) - \tfrac{1}{2}\gamma^2\left[\ell n\,\frac{1}{\eta_0^2} - \left(1 - \eta_0^2\right)\right]\right.$$

$$\left. + \tfrac{1}{2}\Lambda^2\,\eta_0^2\right\} \tag{9.12.1}$$

$$C_P = \frac{\pi}{4}\left(\frac{\kappa + \frac{\Lambda}{2}}{\kappa + \Lambda}\right)^{5/2} (\kappa + \Lambda)\,\gamma\left(1 - \eta_0^2\right) \tag{9.12.2}$$

$$J = \pi\,\kappa\sqrt{\frac{\kappa + \frac{\Lambda}{2}}{\kappa + \Lambda}} \tag{9.12.3}$$

As explained above, the two auxiliary parameters γ and η_0 which occur in these equations are themselves known functions of the two independent parameters κ and Λ. Hence in principle these equations suffice to fix a family of curves of C_F versus J, with C_P as the parameter which changes from one curve to the next.

9.13 Static Thrust and Power Coefficients

The reader can easily verify that under static conditions (V = 0), the foregoing parametric solution reduces to the following form.

$$\varkappa = J = 0 \tag{9.13.1}$$

$$0 \leq \Lambda \leq 1 \tag{9.13.2}$$

$$\gamma = 1 - \sqrt{1 - \Lambda^2} \tag{9.13.3}$$

$$\frac{1}{\eta_0^2} = 1 + \left(\frac{\Lambda}{\gamma}\right)^2 \tag{9.13.4}$$

$$C_F = \frac{\pi^3}{4} \left(\tfrac{1}{2}\right)^2 \left\{ \Lambda^2 \left(1 - \eta_0^2\right) - \frac{\gamma^2}{2} \left[\ell n \frac{1}{\eta_0^2} - \left(1 - \eta_0^2\right) \right] + \tfrac{1}{2} \Lambda^2 \eta_0^2 \right\} \tag{9.13.5}$$

$$C_P = \frac{\pi^4}{4} \left(\tfrac{1}{2}\right)^{5/2} \Lambda \gamma \left(1 - \eta_0^2\right) \tag{9.13.6}$$

Values of C_F , C_P and $C_F/C_P{}^{2/3}$ as calculated from these equations were previously presented in Fig. 2.9.1

9.14 Maximum Attainable Thrust and Power Coefficients

The reader can also readily verify that under the absolute maximum loading limit of Eq. (9.10.8) the general parametric solution reduces to the following simplified results.

$$\Lambda_{MAX} = \sqrt{1 + \varkappa^2} - \varkappa \tag{9.14.1}$$

$$\gamma_{MAX} = 1 \tag{9.14.2}$$

$$\frac{1}{\eta_0^2} = 2 \tag{9.14.3}$$

$$C_F\Big)_{MAX} = \frac{\pi^3}{8}\left\{\tfrac{1}{2}\left[1 + \frac{\kappa}{\sqrt{1+\kappa^2}}\right]\right\}^2\left\{\sqrt{1+\kappa^2}\left(\sqrt{1+\kappa^2} - \kappa\right)\right.$$

$$\left. - (\ell n\ 2 - \tfrac{1}{2}) + \tfrac{1}{2}\left(\sqrt{1+\kappa^2} - \kappa\right)^2\right\} \qquad (9.14.4)$$

$$C_P\Big)_{MAX} = \frac{\pi^4}{8}\left\{\tfrac{1}{2}\left[1 + \frac{\kappa}{\sqrt{1+\kappa^2}}\right]\right\}^{5/2}\sqrt{1+\kappa^2} \qquad (9.14.5)$$

$$J = \pi\kappa\sqrt{\tfrac{1}{2}\left[1 + \frac{\kappa}{\sqrt{1+\kappa^2}}\right]} \qquad (9.14.6)$$

Eq. (9.14.3) shows that under these absolute maximum loading conditions the non-swirling core occupies exactly half the cross-sectional area of the slipstream! Under normal light loadings, the core is of course very much smaller than this.

Curves of $C_F\Big)_{MAX}$ and $C_P\Big)_{MAX}$ versus J as computed from these relations were previously presented in Fig. 2.9.2.

9.15 Relative Flow Angle Downstream of Actuator

In studies relating to pitch setting of variable pitch actuators, it is frequently useful to be able to compute the theoretical relative flow angle β_d at radius r_d on the downstream side of the actuator disc. For the idealized actuator, this is defined by the expression

$$\tan \beta_d = \frac{V_d}{\omega r_d - \frac{\Gamma}{r_d}} \qquad (9.15.1)$$

To relate this to corresponding values in the remote slipstream, we note that

$$r_d = \left(\frac{D}{2R}\right) r = \left[\frac{\mu + \Lambda}{\mu + \frac{\Lambda}{2}}\right]^{\frac{1}{2}} r \tag{9.15.2}$$

$$V_d = \left[\frac{\mu + \frac{\Lambda}{2}}{\mu}\right] V \tag{9.15.3}$$

Upon combining, rearranging and non-dimensionalizing we finally obtain

$$\tan \beta_d = \frac{\sqrt{\frac{\mu + \frac{\Lambda}{2}}{\mu + \Lambda}} \left(\mu + \frac{\Lambda}{2}\right)}{1 - \left(\frac{\mu + \frac{\Lambda}{2}}{\mu + \Lambda}\right) \frac{\nu}{\eta^2}} \tag{9.15.4}$$

The corresponding flow angle β in the remote slipstream itself is given by the simpler expression

$$\tan \beta = \frac{\frac{\mu}{\eta}}{1 - \frac{\nu}{\eta^2}} \tag{9.15.5}$$

Both of these angles vary as functions of η . To find an angle which is respresentative of the pitch setting in some approximate overall sense, it is necessary to use an appropriate mean relative radius η . For example, we may choose as a suitable mean value for this purpose the quantity

$$\eta = \eta_m = \sqrt{\frac{1 + \eta_b^2}{2}} \tag{9.15.6}$$

For an actuator with a sufficiently large number of blades (high blade density) the outlet flow angle β_d at radius η_m will approximately equal the outlet blade angle itself at this point. For larger blade spacings, the relation between flow angle and blade angle is more complex and lies outside the scope of this discussion.

By combining relations (9.15.6) with (9.15.4) and imposing the constraint

$$\beta_d = \text{constant (at radius } \eta_m) \tag{9.15.7}$$

it is possible to find a relation between ν and Λ which corresponds approximately to constant pitch setting (at high blade density). The corresponding values substituted into the general parametric solution of section 9.12 then roughly simulates the performance of an actuator at fixed pitch setting.

10. Dynamic Stability of the Idealized Lifting Rotor in Vertical Ascent or Descent

In this section we consider the response of a lifting rotor to small perturbations from equilibrium. The treatment is deliberately simplified to forcus attention strictly on the basic phenomena. An ideal actuator is assumed, with $P_f = 0$. We analyze a rotorcraft of gross weight W operating in steady vertical climb or descent, except for the imposed perturbations. At the steady reference condition, lift L is equal to weight W. But unlike the weight W which is constant, lift L is subject to small perturbations δL about the equilibrium value. Lift L and weight W are the only forces considered in this analysis, drag and other incidental forces being deliberately ignored.

Under these circumstances it is advantageous to substitute W for L as dimensional reference parameter. Hence we now work in the ρ, D, W dimensional system. The relevant coefficients are defined as follows

$$C_{3P} = \frac{P}{\frac{1}{D}\sqrt{\frac{W^3}{\rho}}} \tag{10.1.1}$$

$$C_{3\dot{H}} = \frac{\dot{H}}{\frac{1}{D}\sqrt{\frac{W}{\rho}}} \tag{10.1.2}$$

$$C_{3L} = \frac{L}{W} \tag{10.1.3}$$

In this system, the fundamental equations for the ideal actuator take the following form -

For Modes P, R and W -

$$C_{3P} = \frac{C_{3L}\, C_{3\dot{H}}}{2} + \sigma_i \sqrt{\left(\frac{C_{3L}\, C_{3\dot{H}}}{2}\right)^2 + \frac{2\tau}{\pi\varphi} C_{3L}{}^3} \tag{10.2.1}$$

For Mode T

$$C_{3P} = -\frac{\pi}{3\sqrt{3}} \tau\, C_{3\dot{H}}{}^3 - C_{3L}\, C_{3\dot{H}} \tag{10.2.2}$$

For the stability analysis it is necessary to find the partial derivatives $\left(\frac{\partial C_{3P}}{\partial C_{3\dot{H}}}\right)$ and $\left(\frac{\partial C_{3P}}{\partial C_{3L}}\right)$. This is easily accomplished by differentiating Eqs. (10.2). However, in the end we require only the equilibrium values of these various quantities. The equilibrium values are obtained simply by setting $C_{3L} = 1$ in the various expressions. Of course, this may be done only <u>after</u> the required differentiations are carried out. In this way the following results are obtained

<u>For modes P, W and R</u> -

$$C_{3P} = \frac{C_{3\dot{H}}}{2} + \sigma_i \sqrt{\left(\frac{C_{3\dot{H}}}{2}\right)^2 + \frac{2\tau}{\pi\varphi}} \tag{10.3.1}$$

$$X = \frac{\partial C_{3P}}{\partial C_{3\dot{H}}} = \frac{1}{2} + \frac{\frac{C_{\dot{H}}}{4}}{\sigma_i \sqrt{\left(\frac{C_{\dot{H}}}{2}\right)^2 + \frac{2\tau}{\pi\varphi}}} \tag{10.3.2}$$

$$Y = \frac{\partial C_{3P}}{\partial C_{3L}} = \frac{C_{\dot{H}}}{2} + \frac{\left[\left(\frac{C_{\dot{H}}}{2}\right)^2 + \frac{3}{\pi}\frac{\tau}{\varphi}\right]}{\sigma_i \sqrt{\left(\frac{C_{\dot{H}}}{2}\right)^2 + \frac{2}{\pi}\frac{\tau}{\varphi}}} \qquad (10.3.3)$$

For mode T -

$$C_{3P} = -\frac{\pi}{3\sqrt{3}}\,\tau\, C_{\dot{H}}^{\,3} - C_{\dot{H}} \qquad (10.4.1)$$

$$X = \frac{\partial C_{3P}}{\partial C_{3\dot{H}}} = -\frac{\pi}{\sqrt{3}}\,\tau\, C_{\dot{H}}^{\,2} - 1 \qquad (10.4.2)$$

$$Y = \frac{\partial C_{3P}}{\partial C_{3L}} = -C_{\dot{H}} \qquad (10.4.3)$$

The basic equations (10.2) can be represented symbolically in the form

$$C_{3P} = C_{3P}\left(C_{3\dot{H}},\, C_{3L}\right) \qquad (10.5.1)$$

Consequently, the small changes occurring during a perturbation may be written

$$\delta C_{3P} = \left(\frac{\partial C_{3P}}{\partial C_{3\dot{H}}}\right) \delta C_{3\dot{H}} + \left(\frac{\partial C_{3P}}{\partial C_{3L}}\right) \delta C_{3L}$$

or

$$\delta C_{3P} = X\ \delta C_{3\dot{H}} + Y\ \delta C_{3L} \qquad (10.5.2)$$

The equation of motion of the rotorcraft during a small perturbation is -

$$\frac{\delta L}{W} = \frac{1}{g}\frac{d}{dt}\left(\delta \dot{H}\right) \qquad (10.6.1)$$

By utilizing the definitions (10.1.2) and (10.1.3) this may be put into the form

$$\delta C_{3L} = \frac{1}{g} \frac{d}{dt} \left[\frac{1}{D} \sqrt{\frac{W}{\rho}} \, \delta C_{3\dot{H}} \right] \tag{10.6.2}$$

It is now advantageous to introduce a non-dimensional time θ defined as follows

$$\theta = \frac{t}{\frac{1}{gD} \sqrt{\frac{W}{\rho}}} \tag{10.6.3}$$

When expressed in terms of this dimensionless time coordinate θ, the equation of motion (10.6.2) becomes simply

$$\delta C_{3L} = \frac{d}{d\theta} \left[\delta C_{3\dot{H}} \right] \tag{10.6.4}$$

It is instructive to include in the analysis the possibility of incorporating an automatic power control system. Specifically, we assume that power input or output may be modulated in response to perturbation velocity and/or acceleration as sensed by appropriate instrumentation. Thus let

$$\delta C_{3P} = - \mu \frac{d}{d\theta} \left[\delta C_{3\dot{H}} \right] - \nu \left[\delta C_{3\dot{H}} \right] \tag{10.7.1}$$

where μ and ν are two non-negative constants representing the response of the control system to perturbation acceleration and perturbation velocity, respectively. Of course, we may set $\mu = \nu = 0$, thus simulating a control system which maintains constant power independently of the state of the motion of the craft.

Upon substituting Eqs. (10.6.4) and (10.7.1) into (10.5.2), we obtain the basic response equation

$$\frac{d}{d\theta}\left[\delta C_{3\dot{H}}\right] = -\left\{\frac{X + \nu}{Y + \mu}\right\}\left[\delta C_{3\dot{H}}\right] \tag{10.8.1}$$

The solution of Eq. (9.8.1) can be taken in the form

$$\left[\delta C_{3\dot{H}}\right] = \left[\delta C_{3\dot{H}}\right]_0 e^{\beta\theta} \tag{10.8.2}$$

$$\frac{d}{d\theta}\left[\delta C_{3\dot{H}}\right] = \beta\left[\delta C_{3\dot{H}}\right]_0 e^{\beta\theta} \tag{10.8.3}$$

Upon substituting these last two expressions into the basic response equation (10.8.2), we finally obtain the result

$$\beta = -\left\{\frac{X + \nu}{Y + \mu}\right\} \tag{10.8.4}$$

where the functions X and Y are as defined in Eqs. (10.3) and (10.4), while μ and ν are two non-negative constants which characterize the control system, if any. Under conditions of constant power input or output, $\mu = \nu = 0$, and Eq. (10.8.4) reduces further to

$$\beta = -\frac{X}{Y} \tag{10.8.5}$$

Stability of operation in vertical ascent or descent requires that β be negative. We shall say that Eq. (10.8.5) defines the inherent stability of the idealized rotor, while (10.8.4) defines the augmented stability.

Study of the actuator derivative functions X and Y as given earlier in Fig. 2.10.1 shows that X is positive for all positive and negative values of the vertical velocity C_{3H}. The function Y, on the other hand, turns out to

be positive for values of $C_{3\dot{H}}$ algebraically greater than $-\frac{3}{\sqrt{\pi}} = -1.693$, and negative for values of $C_{3\dot{H}}$ algebraically less than $-\frac{3}{\sqrt{\pi}}$. This cross-over point coincides with point M on the operating envelope.

We conclude that the ideal lifting rotor is inherently stable over the range

$$-\frac{3}{\sqrt{\pi}} \leq C_{3\dot{H}} \leq +\infty \qquad (10.8.6)$$

This includes all rates of ascent, as well as descent over the full range of power-on reversed thrust operation, and descent over an initial small portion of the windmilling range. It is to be expected that for any real rotor, the range of inherent stability is likely to be considerably more restricted than this.

Eq. (10.8.4) shows very clearly that the range of stable operation can be extended as far below the operating point M as desired simply by introducing the requisite amount of acceleration response as denoted by the constant μ. Note that the velocity response factor ν does not affect the range of stability but merely increases the rate at which disturbances either grow or decay.

Typical stability response curves for various combinations of control parameters as computed from the foregoing equations were shown earlier in Fig. 2.10.2.

11. Actuator Efficiency and Effectiveness

In analyzing the performance of a propeller, windmill or lifting rotor, we are concerned not only with determining the absolute values of force, power and so on, but also with assessing the comparative performance of the device in relation to its theoretical potential. In this connection, an essential first step is to reduce all performance parameters to appropriate dimensionless form since this normalizes the performance of devices of every size and capacity

to a common basis of comparison. However, this first step, while essential, is not necessarily sufficient in itself. For example, to know the actual values of the conventional coefficients C_F, C_P and J in a specific instance is indispensable for some purposes, but nevertheless does not directly indicate the degree of departure from ideal performance. Fortunately, this significant aspect of actuator performance can be expressed simply and consistently by the concept of power loss P_f as defined elsewhere in this paper. Naturally, this loss itself should be expressed in dimensionless form by the coefficient C_f, C_{1f}, C_{2f} or C_{3f} as appropriate, according to the context.

In some cases it is useful to break the total shaft power P down in somewhat more detail as shown, for example, in Table 11.1. From this breakdown of total shaft power P into the four basic components shown, it is possible to define a sequence of significant power ratios as indicated by Eqs. (11.1.1) through (11.2.3) of the table. Note that these definitions all employ the sign changing operator σ_i whose definition is repeated in Eq. (11.4.1). The purpose, of course, is to keep the efficiency and effectiveness ratios as defined in the table always less than unity, regardless of the algebraic sign of the ideal shaft power P_i.

The key relations summarized in Eqs. (11.3) follow at once from the earlier definitions. Notice from Eq. (11.3.3) that the overall power effectiveness e_P is closely related to the power loss coefficient C_{2Pf}.

The familiar concept of efficiency, when applied to actuators, is very useful in some contexts, but completely useless in others. For example, for a propeller operating under cruise conditions, overall efficiency η is ordinarily a factor of prime importance. On the other hand, for a lifting rotor in stationary hovering flight, both η and η_i vanish identically and obviously fail to provide relevant figures of merit. Nevertheless, the power effectiveness

factors e_N, e_r and e_P continue to be significant in this case and do provide useful figures of merit.

Notice that the definition of overall power effectiveness e_P amounts to a comparison of ideal and actual power under conditions of equal thrust. In fact the definition (11.2.3) may be rewritten in equivalent form as

$$e_P = \left[\frac{C_{lPi}}{C_{lP}}\right]^{\sigma_i}_{C_{lF}} \tag{11.5}$$

where the subscript C_{lF} signifies that ideal and actual power coefficients a compared on the basis of equal force coefficient.

It is equally possible, however, to compare the ideal and actual force coefficients on the basis of equal power coefficients for both, and in some situations this is a preferable method of comparison. We recall that for any assigned value of C_{lP}, the ideal actuator has two distinct values of thrust coefficients which we here denote as $C_{lF}\big)_{MAX}$ and $C_{lF}\big)_{MIN}$. At the same value of C_{lP}, the actual thrust coefficient C_{lF} always his within the range

$$C_{lF}\big)_{MIN} \leq C_{lF} \leq C_{lF}\big)_{MAX} \tag{11.6.1}$$

Consequently, there are two significant force ratios which we define as follo namely,

$$e_F = \left[\frac{C_{lF}}{C_{lF}\big)_{MAX}}\right]^{\sigma}_{C_{lP}} \tag{11.6.2}$$

and

$$e_B = \left[\frac{C_{lF}}{C_{lF}\big)_{MIN}}\right]_{C_{lP}} \tag{11.6.3}$$

Notice that the sign changing exponent σ is needed in Eq. (11.6.2) to keep e_F always less than unity regardless of the sign of C_{lP}, but that no sign changing exponent is needed in Eq. (11.6.3). In this connection, recall that $C_{lF})_{MAX}$ has the same sign as C_{lP}, but that $C_{lF})_{MIN}$ is always negative. We may term e_F the thrust effectiveness for positive values of C_{lP}, or the drag effectiveness for negative values of C_{lP}. We may term e_B the braking effectiveness in all cases. This terminology, while arbitrary, is reasonably convenient and clear. The values of e_F or e_B can be readily inferred in any given case from the basic relations presented elsewhere in this paper.

The power loss coefficients, the efficiencies, or the power and force effectiveness ratios defined in this section provide suitable figures of merit for virtually every situation.

Table 11.1 Significant Power Components and Ratios

Components of Total Shaft Power

Component	Sign	Symbol	Subtotals
Thrust Power	$\pm$	FV	P_i
Basic Slipstream Loss	+	P_S	
Idealized Rotation Loss	+	P_N	P_f
Residual Loss	+	P_r	
Total Shaft Power	$\pm$	P	

Significant Power Ratios

$$\eta = \left[\frac{FV}{P}\right]^{\sigma_i} \qquad \text{Overall Efficiency} \qquad (11.1.1)$$

$$\eta_i = \left[\frac{FV}{P_i}\right]^{\sigma_i} \qquad \text{Ideal Efficiency} \qquad (11.1.2)$$

$$e_N = \left[\frac{P_i}{P_i + P_N}\right]^{\sigma_i} \qquad \text{Rotation Power Effectiveness} \qquad (11.2.1)$$

$$e_r = \left[\frac{P_i + P_N}{P}\right]^{\sigma_i} \qquad \text{Residual Power Effectiveness} \qquad (11.2.2)$$

$$e_P = \left[\frac{P_i}{P}\right]^{\sigma_i} \qquad \text{Overall Power Effectiveness} \qquad (11.2.3)$$

Key Relations

$$\eta = \eta_i \, e_P \qquad (11.3.1)$$

$$e_P = e_N \, e_r \qquad (11.3.2)$$

$$e_P = \left[1 - \sigma C_{2Pf}\right]^{\sigma_i} \qquad (11.3.3)$$

(Table continues on next page)

Table 11.1 Cont'd

Sign Changing Operators

$$\sigma_i = \frac{P_i}{|P_i|} = \pm 1 \qquad (11.4.1)$$

$$\sigma = \frac{P}{|P|} = \pm 1 \qquad (11.4.2)$$

12. Bibliography

This paper deals with certain classical fundamentals of fluid mechanics rather than with current research topics in the field. Hence references to the current literature are not involved. However, the analysis presented in this paper does depend heavily on an original approach to dimensional analysis as expounded in the following paper. A further bibliography on dimensional analysis may also be found therein.

"Dimensional Analysis and the Concept of Natural Units in Engineering," T. H. Gawain. Naval Postgraduate School Technical Report NPS-57Gn72031A, March 1972.

DISTRIBUTION LIST

		No. of Copies
1.	Defense Documentation Center Cameron Station Alexandria, Virginia 22314	20
2.	Library Code 0212 Naval Postgraduate School Monterey, California 93940	2
3.	Provost Code 02 Naval Postgraduate School Monterey, California 93940	1
4.	Dean of Research Code 023 Naval Postgraduate School Monterey, California 93940	1
5.	Professor T. J. Williamson Chairman, Research Committee Code 61 Naval Postgraduate School Monterey, California 93940	1
6.	Chairman Department of Mechanical Engineering Code 59 Naval Postgraduate School Monterey, California 93940	1
7.	Chairman Department of Aeronautics Code 57 Naval Postgraduate School Monterey, California 93940	1
8.	Professor J. A. Bennett Code 57Zn Naval Postgraduate School Monterey, California 93940	1
9.	Professor T. H. Gawain Code 57Gn Naval Postgraduate School Monterey, California 93940	50

10. Dr. E. S. Lamar
Naval Air Systems Command
Washington, D. C. 20360 — 1

11. Dr. H. J. Mueller
Naval Air Systems Command
Washington, D. C. 20360 — 1

12. Technical Library
Naval Air Systems Command
Washington, D. C. 20360

13. Code 031
Naval Ships System Command
Washington, D. C. 20360 — 1

14. Technical Library
Naval Ships System Command
Washington, D. C. 20360 — 1

15. Dr. Morton Cooper
Code 438
Office of Naval Research
Washington, D. C. 20360 — 1

16. Dr. Ralph Roberts
Code 473
Office of Naval Research
Washington, D. C. 20360 — 1

17. Technical Library
Office of Naval Research
Washington, D. C. 20360 — 1

18. Dr. J. W. Schott
Naval Ship Research and Development Center
Carderock, Maryland — 1

19. Dr. H. J. Lugt
Naval Ship Research and Development Center
Carderock, Maryland — 1

20. Technical Library
Naval Ship Research and Development Center
Carderock, Maryland — 1

21. Technical Library
U. S. Naval Weapons Laboratory
Dahlgren, Virginia 22448 — 1

22. Technical Library
U. S. Naval Academy
Annapolis, Maryland 21402 — 1

23. Technical Library
National Aeronautics & Space Administration
Washington, D. C. 20360 — 1

24. Technical Library
National Aeronautics & Space Administration
Lewis Research Center
Cleveland, Ohio 44121 — 1

25. Technical Library
National Aeronautics & Space Administration
Ames Research Center
Moffett Field, California 94035 — 1

26. Dr. Hans Von Ohain
Wright-Patterson Air Force Base
Dayton, Ohio 45433 — 1

27. Technical Library
Wright-Patterson Air Force Base
Dayton, Ohio 45433 — 1

28. Dr. G. L. Hollingsworth
Technical Director
Naval Air Development Center
Warminster, Pa. 18974 — 1

DOCUMENT CONTROL DATA - R & D

(Security classification of title, body of abstract and indexing annotation must be entered when the overall report is classified)

1. ORIGINATING ACTIVITY (Corporate author)	2a. REPORT SECURITY CLASSIFICATION
Naval Postgraduate School Monterey, California 93940	UNCLASSIFIED
	2b. GROUP None

3. REPORT TITLE

Generalized Performance Limits for Propellers, Windmills and Lifting Rotors with Axes Parallel to the Undisturbed Flow

4. DESCRIPTIVE NOTES (Type of report and inclusive dates)

Technical Report, 1972

5. AUTHOR(S) (First name, middle initial, last name)

Theodore H. Gawain

6. REPORT DATE	7a. TOTAL NO. OF PAGES	7b. NO. OF REFS
December 1972	101	1

8a. CONTRACT OR GRANT NO.	9a. ORIGINATOR'S REPORT NUMBER(S)
b. PROJECT NO.	NPS-57Gn72121A
c.	9b. OTHER REPORT NO(S) (Any other numbers that may be assigned this report)
d.	

10. DISTRIBUTION STATEMENT

This document has been approved for public release and sale; its distribution is unlimited.

11. SUPPLEMENTARY NOTES	12. SPONSORING MILITARY ACTIVITY

13. ABSTRACT

This paper generalizes the classical momentum theory as usually applied to propellers, windmills and lifting rotors into a single unified treatment. It also extends the analysis to include the regime in which flow through part or all of the actuator disc is reversed with respect to the remote flow field. Dimensional analysis is used in a systematic manner to reduce the final results to their simplest and most significant forms. It is shown that the performance of these devices can always be represented by a single parameter family of curves in which the parameter expresses the extent to which the performance of the actual device falls short of the theoretical limit. Detailed algebraic solutions are derived in closed form for the performance of both the idealized zero torque and finite torque actuators; these represent performance limits which any comparable real device may approach but never exceed. A qualitative analysis is presented concerning the development of the vortex ring state. The fundamental dynamic stability of the ideal lifting rotor is also analyzed.

While this paper deals with a classical topic in fundamental fluid mechanics, the approach employed is original and many of the results derived here are in a form that is essentially new. In particular, the solutions obtained for the reversed and transition flow regimes and for the idealized rotating actuator are believed to represent new formulations of these basic phenomena.

14 KEY WORDS	LINK A		LINK B		LINK C	
	ROLE	WT	ROLE	WT	ROLE	WT
Propellers						
Axial turbines						
Windmills						
Lifting rotors						
Helicopters						
Fans						
Performance coefficients						
Performance limits						
Momentum theory of propellers						
Actuator disc						
Vortex ring state of lifting rotor						
Stability of lifting rotor						
Thrust						
Drag						
Power						
Efficiency						
Effectiveness						
Figures of merit						
Dimensional analysis						